Cholinergic agonist PNU282987 induces pro-inflammatory gene expression via the MCOLN1-TFEB pathway in murine macrophages.

Havisha H. Honwad[1,2], Mehran Najibi[3], Balazs Koscso[4,5], Milena Bogunovic[4], Javier E. Irazoqui[1*]

[1] Department of Microbiology and Physiological Systems and

[2] Immunology & Microbiology Program, University of Massachusetts Chan Medical School, Worcester, USA

[3] Department of Pathology, New York University Grossman School of Medicine, New York, USA

[4] Department of Pathology, University of Massachusetts Chan Medical School, Worcester, USA

[5] Obsidian Therapeutics, Cambridge, USA

*Correspondence: Javier.Irazoqui@umassmed.edu

ABSTRACT

Neurotransmitter signaling in macrophages is a modulatory mechanism during inflammation. Treatment of macrophages with acetylcholine, or agonistic molecules carbachol and PNU282987, considered to be specific for the Alpha7 nicotinic ACh receptor (α7NAChR), represses cytokine expression in inflammatory disease models, leading to the idea that α7NAChR stimulation could modulate inflammation in health and disease. However, their

effects on resting macrophages are largely unaddressed. This study assesses the impact of PNU282987 on macrophage phenotypes *in vitro*, focusing on bone marrow-derived macrophages (BMDMs) and RAW264.7 cells. We found that PNU282987 induces a specific pro-inflammatory gene expression profile, elevating *Ifnb1, Il1b, Il6,* and *Tnf* levels. However, this did not translate to increased cytokine secretion. Unexpectedly, both BMDM and RAW264.7 cells showed no detectable α7 nicotinic acetylcholine receptor expression, challenging the proposed action mechanism of PNU282987. Instead, our data suggest a non-receptor-mediated pathway, where PNU282987 may activate the stress-responsive TFEB transcription factor via ROS generation, implicating the MCOLN1-calcineurin pathway. Our findings reveal that the primary action of PNU282987 in resting macrophages is through non-receptor-mediated pro-inflammatory gene expression and TFEB activation, offering new insights into its pharmacological effects beyond the conventional receptor-based mechanisms.

INTRODUCTION

The neurotransmitter acetylcholine (ACh) modulates inflammatory responses in what is known as the cholinergic anti-inflammatory pathway (CAIP) (1, 2). Nicotinic ACh receptors composed of α7 subunits (α7NAChR) expressed in macrophages have been implicated in mediating the CAIP (3, 4), mainly through inhibition of NF-κB activity (5, 6). Exactly how α7NAChR represses NF-κB is not completely understood, but the mechanism appears to include a JAK2/STAT3 pathway (7). Nonetheless, α7NAChR activation has been proposed as a therapeutic strategy for several inflammatory diseases, including sepsis (8, 9), ulcerative colitis (10, 11), arthritis (12, 13), lung inflammation (14, 15), cystic fibrosis (16), Type 2 diabetes (17, 18), and Parkinson's disease(19). α7NAChR agonists, such as PNU282987, have been used to suppress pro-inflammatory responses of various cell types, including macrophages, in models for these

diseases (5, 7, 20, 21). PNU282987, a selective α7NAChR agonist (22, 23) has been shown to protect against sepsis or LPS induced lung injury (24-26) or alleviate DSS-induced colitis inflammation (27) by inhibiting inflammatory mediators in model systems. Nonetheless, to therapeutically deploy α7NAChR agonists to treat inflammation, it is necessary to understand their effects on cells in their resting state, yet these are vastly understudied. Importantly, it is currently unknown if α7NAChR agonists trigger cellular stress, which could affect their safety profiles.

Transcription factor EB (TFEB) is a sensitive reporter of cell stress. Known as a master regulator of lysosome biogenesis and autophagy regulation (28, 29), TFEB was recently shown to participate in the integrated stress response (30, 31). When activated by starvation, infection, or oxidative stress, TFEB translocates from the cytosol into the nucleus to drive gene expression (32-36). Although TFEB is broadly expressed in mice and humans, its downstream target genes appear to be largely cell type-specific through unknown mechanisms (37). Importantly, understanding of TFEB functions in macrophages is in its infancy.

To better understand the effects of α7NAChR agonists on innate immunity, we examined PNU282987-treated murine bone marrow-derived macrophages (BMDMs) and a macrophage-like cell line. Surprisingly, PNU282987 drove a pro-inflammatory gene expression program in both systems, despite a lack of convincing evidence of α7NAChR expression in these cells. As an alternative mechanism of action, we found that PNU282987 triggered TFEB activation in both cell types, and that the pro-inflammatory response was highly TFEB-dependent. Moreover, we detected higher levels of reactive oxygen species (ROS) in PNU282987-treated cells compared to controls, suggesting that PNU282987 might activate TFEB by oxidative stress.

66 Further analysis of the previously described ROS-MCOLN1-calcineurin pathway of TFEB
67 activation (38) was consistent with this alternative mechanism of action.

68 **MATERIALS AND METHODS**

69 **Mice**

70 Mouse colony maintenance and procedures were performed in accordance with the Guidelines
71 for the Care and Use of Laboratory Animals, published by the US National Institutes of Health,
72 and were approved by the Institutional Animal Care and Use Committee (IACUC) of the
73 University of Massachusetts Chan Medical School. Wild type mice, Strain: C57BL/6J (Stock #:
74 000664) and *Chrna7*$^{-/-}$ mice, Strain: B6. 129S7-*Chrna7*^{tm1Bay}/J (Stock #: 003232) mice were
75 ordered from The Jackson Laboratory. *Tfeb*$^{fl/fl}$ mice were a gift from Dr. Andrea Ballabio,
76 TIGEM, Naples, Italy (29). Tfebfl/fl *LysM-Cre*$^{\pm}$ mice were bred in house (38). BMDM
77 genotyping for wild type and *Chrna7*$^{-/-}$ BMDMs was performed by following steps described in
78 Protocol 28408: Standard PCR Assay - Chrna7<tm1Bay>-Alternate 1 for Jackson lab stock No:
79 003232.

80 **Isolation and differentiation of primary murine BMDMs**

81 Bone marrow cells were isolated from separated femurs and tibias from euthanized 8-12-week-
82 old mice as previously described (38). Isolated bone marrow cells from C57BL/6, *Chrna7*$^{-/-}$,
83 *Tfeb*$^{fl/fl}$ and *Tfeb*$^{\Delta LysM}$ mice were cultured in BMDM differentiation medium: DMEM containing
84 4.5 g/L glucose, L-glutamine (Corning, 10-013-CV), sodium pyruvate supplemented with 20%
85 conditioned medium from L929 cells, 10% FBS, 1% AA for 7 days. Cells were seeded in non-
86 tissue culture treated Petri dishes (Fisherbrand, FB0875712) and incubated at 37°C, in a
87 humidified chamber with 5% CO_2. Cells were seeded for experiments after 7 days of
88 differentiation.

89 **Cell culture and transfection**

90 G418 sulfate (Life Technologies, 10131) was used for selection and stable cells were selected by
91 FACS 10 days after selection. RAW264.7 and *Tfeb*$^{-/-}$ *Tfe3*$^{-/-}$ RAW264.7 cells, a gift from Dr.
92 Rosa Puertollano, NHLBI (39) and iBMDMs (38) were grown in Dulbecco's Modified Eagle's
93 Medium (DMEM) containing 4.5 g/L glucose, L-glutamine (Corning, 10-013-CV), sodium
94 pyruvate supplemented with 10% Fetal Bovine Serum (FBS; Gibco, 16000044) and 1%
95 Antibiotic-Antimycotic (Gibco, 15240062). Cells were grown at conditions of 37°C, in a
96 humidified chamber with 5% CO_2 and passaged 4 to 10 times.

97 **Drugs and Reagents**

98 PNU282987 (Sigma-Aldrich, P6499) powder form was carefully dissolved in DMSO (Sigma-
99 Aldrich, D2438) - sterile, filtered, cell culture grade, Bio Performance certified, meets EP and
100 USP specifications thus, devoid of endotoxin or pro-inflammatory contaminants; Carbachol
101 (Sigma-Aldrich, 212385); MG624 Cayman Chemical Company, 24298); LPS from *S. enterica*
102 serotype Typhimurium (Sigma-Aldrich, L6143-1 MG); Torin-1 (Tocris, 427); FK-506 (Cayman
103 Chemical Company, 10,007,965); BAPTA-AM (Cayman Chemical Company, 15,551); kb-NB-
104 142-70 (Cayman Chemical Company, 18,002); α-bungarotoxin Alexa Fluor 647 conjugate
105 (Thermo Fisher Scientific, B35450)

106 **Immunofluorescence and fluorescence imaging**

107 Cells were seeded in 96-Well Optical Bottom Plates (Thermo Scientific, 165305) and incubated
108 overnight to attain cell confluency of 0.06 x 10^6 for experiments. Following experiments with
109 iBMDM GFP-TFEB cells, fixation step was performed using 4% paraformaldehyde (PFA)
110 (Sigma Aldrich, 158127) and cells were incubated with Hoechst stain (Anaspec, AS-83218) for
111 20 min at room temperature as nuclear staining. For immunofluorescence, cells were washed 3

112 times with PBS (Gibco Life Technologies,10010) for 5 min, permeabilized with 0.1% Triton X in
113 PBS at on shaker at room temperature for 5 min, washed 3 times with PBS and blocked with 5%
114 bovine serum albumin (Sigma Aldrich, A9647) in PBS for 1 h. After washing with PBS (3
115 times), cells were incubated with primary antibody for 2 h Anti-TFEB Antibody (Abcam,
116 ab2636). After washing 3 times in PBS, cells were incubated with the fluorescently labelled
117 secondary antibody (Thermo Fisher Scientific, A11058) along with Hoechst stain (Anaspec, AS-
118 83,218) for 1 h at room temperature. For LysoTracker staining, cells were incubated with 100
119 nM LysoTracker DND-99 (Thermo Fisher, L7528) added to cell culture media for 30 min before
120 fixation step, according to manufacturer's instructions. Image acquisition for calculating TFEB
121 N:C ratio and for Lysotracker mean fluorescence intensity (MFI) was performed using Lionheart
122 FX automated microscope (Biotek) and Gen5 software (version 3.13).

123 **Determination of N:C ratio**

124 Nucleus to cytoplasm (N:C) ratio for TFEB was measured using CellPofiler (40), following our
125 previously described protocol (38). In brief, we used the 3_channels_pipeline.cppipe. which
126 uses nuclear stain (Hoechst) as primary object or "seed" region for building image segmentation
127 masks to distinguish individual cells by marking boundaries, define subcellular regions and
128 generate specific fluorescent intensity values. The pipeline calculated N:C ratio as mean
129 fluorescent intensity of nucleus relative to mean fluorescence intensity of the cytosol.

130 **RT-qPCR**

131 Cells were lysed using Trizol Reagent (1 mL per 1.5 ml microcentrifuge tube). 100 µL
132 chloroform was added and samples were centrifuged at 12,000 rpm to separate the RNA
133 containing aqueous phase. The aqueous layer was transferred to Purelink RNA mini kit column
134 and total RNA was extracted according to manufacturer's instructions. cDNA was prepared using

135 iScript gDNA clear cDNA synthesis kit (Bio-Rad, 1725035). Diluted cDNA was used for RT-
136 qPCR, performed using SYBR Freen Super mix (Bio-Rad) and ViiA7 Reat-Time qPCR system
137 (Applied Bioscience). CT values were obtained for test genes and relative expression was plotted
138 following normalization to reference gene *Gapdh*.

139 **RNA sequencing and differential expression analysis**

140 BMDMs differentiated from WT, *Chrna7*$^{-/-}$, *Tfeb*$^{fl/fl}$, *Tfeb*$^{\Delta LysM}$ mice were treated with DMSO
141 control or PNU282987 (50 µL) for 2 h. Total RNA was extracted from samples as described
142 above using Purelink RNA mini kit (Thermo Fisher Scientific, 12183018A). Whole cell RNA
143 from 4 replicates per condition were sent to Azenta/ Genewiz for polyA selection, library
144 preparation and sequencing using Illumina Nova-Seq or HiSeq platform, 2x150bp, ~350M PE
145 reads. Azenta/Genewiz provided raw data in the form of reads in FASTQ format. FASTQ files
146 were analyzed using the RNA-seq pipeline (Version 1.6.0) on ViaFoundry software (V1.6.5)
147 (41). Using the pipeline, FASTQ paired end reads were trimmed, quality filtered by FastQC,
148 followed by 3' adapter sequence removal and aligned to *Mus musculus* reference genome mm10
149 using STAR and RSEM was used to estimate gene and isoform levels. DEBrowser (v1.28.0) was
150 used for gene count normalization, data analyses, generate visual graphs of differentially
151 expressed genes like volcano plots. Differentially expressed gene sets were considered
152 significant for fold change ≥ 1.5; Padj ≤ 0.01 and were used as input for g:Profiler (42).
153 Comparison of DE genes with public GEO RNA-Seq datasets was performed using Enrichr, a
154 web-based tool used for enrichment analysis that compares gene lists with gene set libraries of
155 known biological function (43). Venn diagrams were made using DeepVenn (44).

156 **ELISA**

157 Secreted levels of TNF-α (DY410-05), IL-1β (DY401-05), IL-6 (DY406-05), IFN-β (DY8234-
158 05), IL-10 (DY417-05), TNFSF15 (DY-1896) were measured using kits purchased from R&D
159 Systems. Briefly, 96-well plates were coated with capture antibody and incubated at room
160 temperature overnight. Plates were washed with Tris buffered saline (TBS) with 0.5% Tween 20
161 (Bethyl Laboratories, E106). Wells were blocked for 1 h with Reagent Diluent - TBS containing
162 1% bovine serum albumin (BSA) (Bethyl Laboratories, E106). After washing, samples or
163 standards diluted in Reagent Diluent were added and plates were incubated for 2 h at room
164 temperature. Detection antibody was added following washing and plates were incubated for 2 h.
165 After washing, Streptavidin-horseradish peroxidase (Strep-HRP) was added for 20 min. TMB
166 One Component HRP Microwell substrate (Bethyl Lab, E102) was added, and reaction was
167 stopped using ELISA Stop Solution (Bethly Laboratories, E115) Optical density (OD) was
168 measured immediately at 450 nm as well as 540 nm using a SpectraMax Plus 384 Microplate
169 Reader with Softmax Pro software. OD measured at 540 nm was subtracted from 450 nm to
170 correct for optical imperfections as per manufacturer's guidelines. Concentrations of the samples
171 (pg/μL) were interpolated from respective standard curve using GraphPad Prism 10.

172 **Cell viability assay**

173 Cell viability was determined using CellTiter-Glo 2.0 Assay (Promega, G7570), according to the
174 manufacturer's instructions. Luminescence was measured using Biotek Synergy H4 Plate Reader
175 Gen5 (version 3.14).

176 **ROS/Superoxide detection assay**

177 Cellular ROS/Superoxide Detection Assay Kit (Abcam, ab139476) was used according to
178 manufacturer's instructions. Mean fluorescence intensity (MFI) was visualized on a Lionheart
179 microscope (Biotek) and measured using Gen5 Data Analysis Software (Version 3.13).

180 **siRNA knockdown**

181 siRNA reagents were purchased from Dharmacon RNAi Technologies: siGENOME
182 NonTargeting siRNA #1 (D-001210-01-05), siGENOME Mouse *Ppp3cb* (19,056) siRNA (M-
183 063545-00-0005), siGENOME Mouse *Ppp3r1* (19,058) siRNA (M-040744-01-0005),
184 siGENOME Mouse *Mcoln1* (94178) siRNA (M-044469-00-515 0005). For transfection, we used
185 Lipofectamine RNAiMAX (Thermo Scientific, 13,778,030), according to manufacturer's
186 instructions.

187 **Western Blotting**

188 Cell samples were washed 3 times with PBS, harvested, and lysed with 1X SDS sample buffer
189 Blue Loading Pack (Cell Signaling Technology, 7722) at 100 µl per well of 6-well plate. Lysates
190 were heated at 100°C for 5 min and then centrifuged for 5 min. The supernatant was collected
191 and sonicated, gel electrophoresis was performed using Novex 4–20% Tris-Glycine Mini Gels
192 (Invitrogen, XP04200BOX), and were then transferred onto nitrocellulose (Life Technologies,
193 LC2009). After washing with TBS (Life Technologies, 28,358) for 5 min, membranes were
194 soaked in blocking buffer containing 1X TBS with 5% BSA for 1 h at room temperature. After 3
195 washes with TBS-Tween 20 (Life Technologies, 28,360), membranes were incubated overnight
196 at 4°C with primary antibodies and gentle agitation. Next, membranes were washed thrice with
197 TBS-Tween 20 and incubated with HRP-conjugated secondary antibody (Cell Signaling
198 Technology, 7074 1:2000) for 1 h at room temperature with gentle agitation. Membranes were

199 then washed with TBSTween20 and incubated with LumiGLO® (Cell Signaling Technology,
200 7003) for 1 min and imaged using Gel box imager (Syngene) GeneSys software. Primary
201 antibodies and dilutions were as follows: ACTB/β-actin antibody (Cell Signaling Technology,
202 4967; 1:1000), α7nAChR antibody (Abcam ab216485, 1:500)

203 **α-bungarotoxin staining and flow cytometry**

204 α-bungarotoxin, Alexa Fluor 647 Conjugate (Thermo Fisher Scientific, B35450) was used
205 according to manufacturer's guidelines to stain murine peritoneal macrophages and muscularis
206 macrophages, isolated according to previously described methods (45) by flow cytometry-based
207 cell sorting (46). Data were analyzed by FlowJo.

208 **Mouse whole brain lysate for Western Blot**

209 In brief, Frozen brain tissue from adult 9-month-old C57Bl/6J mice were homogenized in Cell
210 Lysis Buffer (EPX-99999-000) and centrifuged at 4°C for 20 min at 18000 x *g* to obtain brain
211 lysate.

212 **Determination of bactericidal activity**

213 *Escherichia coli* DH5α was purchased (ThermoFisher Scientific,18265017). *Staphylococcus*
214 *aureus* NCTC8325 is a gift from Fred Ausubel, MGH Research Institute, USA. Bacteria were
215 grown overnight at 37°C in TSB (Sigma-Aldrich, T8907) supplemented with 10 μg/ml nalidixic
216 acid for *S. aureus*, or LB medium (Fisher Scientific, BP1425-500) for E. coli DH5α. Cultures
217 were diluted 1:50 in the respective media the next day and grown at 37°C to mid-exponential
218 phase. WT and *Tfe3 Tfeb* dKO RAW 264.7 cells were infected with *S. aureus* (MOI = 10) and
219 DH5α *E. coli* (MOI = 50) and incubated at 37°C for 30 mins as previously described (38).
220 Lysates were serially diluted, aliquots were plated on TSA (Difco, BD, 236,950)-nalidixic acid

agar (*S. aureus*) or LB agar (*E. coli*) and incubated overnight at 37°C, and colonies were counted for colony-forming units/ml calculation.

Statistical analysis

Quantitative data comparisons were analyzed using statistical tests, performed as indicated in each Figure Legend. $P \leq 0.05$ were judged to be significant. For normally distributed data and comparisons with a single condition, we used the two-sample two-sided t-test. For multiple comparisons, we used one-way ANOVA followed by Tukey's post-hoc test and Two-way ANOVA and Sidak's multiple comparison tests.

RESULTS

PNU282987 induces bone marrow-derived macrophages to express pro-inflammatory genes

To understand the effects of PNU282987 treatment on macrophage phenotype, we exposed *in vitro*-differentiated bone marrow-derived macrophages (BMDMs) to 50 μM PNU282987 for 2 h. We chose an early timepoint of exposure to focus on the initial primary response triggered by this treatment and to avoid secondary effects due to long-term treatment. Immediately following 2 h exposure, we collected RNA and performed RNA-seq to identify differentially expressed genes between PNU282987-treated cells and DMSO-treated control. PNU282987-treated cells showed 572 induced genes and 119 repressed genes (**Fig. 1A, Table S1**). The induced genes were enriched for various KEGG pathways, most of which were related to pro-inflammatory signaling (*e.g.* "TNF signaling pathway", "Cytokine-cytokine receptor interaction", "NF-κB signaling pathway", and "Lipid and atherosclerosis", **Fig. 1B** and **Table S2**). Consistently, complementary Gene Ontology (GO) and Reactome enrichment analyses also showed enrichment of pro-inflammatory categories (**Table S2**). In contrast, the repressed genes

were not significantly enriched for any KEGG pathways or GO categories. These results suggested that PNU282987 induced a pro-inflammatory gene expression profile in BMDMs.

Among the induced genes, *Ifnb1, Il1b, Il6, Tnf* and *Il10* stood out. These genes encode the precursors for cytokines IFN-β1, IL-1β, IL-6, TNF-α and IL-10 respectively, which are key regulators of inflammation. To test if the induced mRNA expression resulted in enhanced cytokine production, we performed ELISA of culture supernatants from BMDMs treated with PNU282987 for 12 h to allow for protein production and secretion. This PNU282987 treatment did not induce the secretion of any of the cytokines (**Fig. 1C-G**). PNU282987 also did not cause measurable lactate dehydrogenase (LDH) release (**Fig. 1H**), ruling out cell death as a reason for the lack of cytokine secretion.

In contrast, PNU282987 had a marked effect on cytokine secretion of LPS-primed macrophages. After stimulation with LPS for 12 h, secretion of IL-6, TNF-α, and IFN-β1 was elevated (**Fig. 1C-E**). Subsequent PNU282987 treatment after LPS stimulation strongly inhibited IL-6 secretion, but not that of TNF-α and IFN-β1 (**Fig. 1C-E**). PNU282987 treatment for 2 h prior to LPS stimulation again only inhibited IL-6 (**Fig. 1C-E**). These results showed that PNU282987 inhibits LPS-stimulated IL-6 secretion under both regimens, consistent with prior reports of anti-inflammatory activity for PNU282987 in LPS-stimulated macrophages (24, 47). Taken together, the data reveal that PNU282987 elicits an early pro-inflammatory gene expression profile in macrophages that does not result in enhanced cytokine secretion. In the context of LPS stimulation, PNU282987 prophylactically or therapeutically reduced LPS-induced IL-6.

To verify these results in an alternative *in vitro* model, we used RAW264.7 cells, a murine macrophage-like cell line. Similar to our observations with wild type BMDMs, PNU282987 treatment for 2 h induced a clear pro-inflammatory gene signature (**Fig. S1A, B and Table S3**). The induced pro-inflammatory genes included *Ifnb1, Il1b, Il6,* and *Tnf,* as was the case with BMDMs. Also consistent with our BMDM results, PNU282987 treatment did not drive secretion of IL-6, TNF-α, IFN-β1, or IL-1β after 12 h (**Fig. S1C-F**). Thus, in RAW264.7 cells as in BMDMs, PNU282987 treatment induced an early pro-inflammatory gene expression profile that did not result in secretion of pro-inflammatory cytokines.

In RAW264.7 cells, LPS stimulation elicited IL-6 and TNF-α secretion (**Fig. S1C-F**). Prior PNU282987 treatment partially inhibited IL-6, TNF-α, and IFN-β1 secretion, and PNU282987 treatment after LPS stimulation did not significantly change levels of IL-6, TNF-α and IFN-β1. Over the same time scale, PNU282987 induced the same 240 genes in BMDMs and RAW264.7 cells (**Fig. S1G**). These overlapping genes were enriched for pro-inflammatory genes, especially those related to TNF signaling (**Fig. S1H**). This is likely a direct effect, since PNU282987 did not induce TNF-α secretion. Taken together, these results establish that PNU282987 induces pro-inflammatory gene expression programs in two distinct *in vitro* macrophage models.

BMDMs and RAW264.7 cells do not express detectable levels of acetylcholine receptors

The proposed mechanistic target of PNU282987 is the α7 nicotinic acetylcholine receptor (α7NAChR) (23). However, direct evidence of α7NAChR expression in *in vitro* and *in vivo* macrophage models is limited. To measure expression of α7NAChR, we performed RT-qPCR using previously published (47, 48) as well as newly designed oligonucleotide primers, and measures *Chrna7* gene expression RNA samples from wild type and *Chrna7*$^{-/-}$ mice (49). These

approaches showed robust *Chrna7* expression in wild type brain lysate controls (**Fig. 2A**). In contrast, the same approach did not show *Chrna7* expression in wild type BMDMs and did not show significant differences with *Chrna7*$^{-/-}$ BMDMs (**Fig. 2B**). Similarly, we did not detect significant expression of nicotinic receptor subunits (α3, α4, α5, α6, α9, α10, β3, and β4) or muscarinic receptors (M1, M2, M3, M4, M5) in either background (**Fig. 2C**). We detected variable low expression of β2 nicotinic receptor subunit which showed significant difference between wild type and *Chrna7*$^{-/-}$ BMDMs (**Fig. 2C**). Thus, at the transcript level we did not obtain convincing evidence of α7NAChR expression in BMDMs.

We used immunoblotting to detect α7NAChR in whole cell lysates using an anti-α7NAChR antibody that was previously used for the same application (50, 51). We used *Chrna7*$^{-/-}$ BMDMs as negative controls, genotyped to ensure their identity (**Fig. S2A**). Immunoblots showed several bands, but no differences between wild type and *Chrna7*$^{-/-}$ (**Fig. S2B**). Thus, we did not obtain convincing evidence of α7NAChR protein expression.

Fluorescently labelled α-bungarotoxin has been used to detect α7NAChR surface expression in THP-1 macrophage cells, monocyte derived macrophages and murine intestinal macrophages (52-54). α-bungarotoxin staining of primary murine peritoneal macrophages and intestinal macrophage populations isolated from small and large bowel of wild type mice (45) yielded negative results for α7NAChR expression (**Fig. S3-S6**). Additionally, we were unable to detect α7NAChR expression by immunofluorescence staining using α7NAChR antibody (not shown). Thus, by three orthogonal approaches and in multiple macrophage cell types, we were unable to detect the expression of α7NAChR. Moreover, Immgen (**Fig. S7A**) and the Human Protein Atlas (**Fig. S8A**) report that both mRNA and protein levels are undetectable in murine

and human macrophages. These data called into question the mechanism of action of PNU282987.

Chrna7$^{-/-}$ BMDMs are defective in the transcriptional response to PNU282987

Given our lack of evidence of α7NAChR expression, we tested the role of α7NAChR genetically. Mice deleted for *Chrna7* were generated previously (49). We used RNA-seq to measure the PNU282987-induced response in *Chrna7*$^{-/-}$ BMDMs. Compared to vehicle control, PNU282987 treatment induced the expression of just 12 genes in *Chrna7*$^{-/-}$ BMDMs (including *Tnf, Fnip2, Gng4, Rragd)* (**Fig. S2C, Table S4**). Thus, the response to PNU282987 was blunted in *Chrna7*$^{-/-}$ BMDMs.

Compared to wild type BMDMs, PNU282987-treated *Chrna7*$^{-/-}$ BMDMs did not induce 564 genes that were induced in wild type BMDMs. Only 8 genes were induced in both backgrounds (**Fig. 2D** and **Table S5**). Direct comparison of the transcriptomes of PNU282987-treated wild type and *Chrna7*$^{-/-}$ BMDMs showed that the vast majority of the innate immune signaling and pro-inflammatory gene changes were only induced in the wild type (**Fig. 2E, F** and **Table S6**). On the other hand, PNU282987-treated *Chrna7*$^{-/-}$ BMDMs differentially expressed genes related to Ras and Rap1 signaling and the lysosome (**Table S6**). These results suggested that *Chrna7*$^{-/-}$ BMDMs lack the PNU282987-induced pro-inflammatory transcriptional response.

To better understand why *Chrna7*$^{-/-}$ BMDMs exhibited such a strongly defective response to PNU282987, we examined gene expression comparing DMSO-treated control BMDMs given the uncertainty of α7NAChR mediating PNU282987 induced response. Expression of genes encoding macrophage markers CD11a, CD11c, CD14 and MHC Class II showed significant differences between wild type and *Chrna7*$^{-/-}$ BMDMs, while other macrophage marker genes

(genes encoding for CD15, CD16, CD64, CD32, F4/80, CD33, CD68, CD80, and CD86) did not show significant differences (**Fig. S2D, Table S7**). These results ruled out a broad defect in macrophage *in vitro* differentiation.

Compared to wild type at baseline, *Chrna7*$^{-/-}$ BMDMs showed decreased expression of many immune-related genes, such as *Il6, Il1a, Il1b, Cxcl2*, and *Nox1* (Fig. S2E, F, G and **Table S8**). These results showed that *Chrna7*$^{-/-}$ BMDMs show significant differences in the expression of a large number of immunity-related genes at baseline, which in itself may cause an altered response to PNU282987.

PNU282987 activates innate immunity and stress-response transcription factor TFEB

Given the lack of α7NAChR expression on BMDMs and the broad defect in innate immune gene expression in *Chrna7*$^{-/-}$ BMDMs, we considered an alternative hypothesis for the pro-inflammatory response to PNU282987: namely, the induction of cellular stress. To detect cellular stress, we examined transcription factor TFEB, which participates in the integrated stress response, as shown in mouse embryonic fibroblasts and retinal pigment epithelial cells (30). TFEB resides in the cytosol in an inactive state. Under stressful conditions, including nutrient deprivation (29, 32), oxidative stress (55, 56), and pathogen infection(35, 38), TFEB translocates to the nucleus and drives the expression of autophagy, lysosomal, and immune genes. Thus, nuclear accumulation of TFEB can serve as a sensitive indicator of cell stress.

To determine TFEB translocation, we measured the ratio of nuclear and cytosolic TFEB staining (N/C ratio) by immunofluorescence microscopy in cells that were treated with PNU282987 and the commonly used α7NAChR inhibitor, MG624 (57, 58). Resting wild type BMDMs showed low nuclear staining (**Fig. 3A, G**). Treatment with PNU282987 modestly but

significantly increased TFEB nuclear localization (**Fig. 3B, G**), which was slightly but significantly inhibited by MG624 pretreatment (**Fig. 3D, G**).

To probe the specificity of this response, we used carbachol, which is a broad-spectrum cholinergic agonist (59-61). Carbachol treatment more strongly increased TFEB nuclear localization (**Fig. 3E, H**). Moreover, MG624 pretreatment completely suppressed TFEB translocation (**Fig. 3F, H**). MG624 treatment, alone or in combination, suppressed TFEB expression, judging by the overall staining intensity of MG624-treated cells compared to DMSO controls (**Fig. 3A, C, D, F**). Thus, although MG624 is considered a specific α7NAChR inhibitor, it also reduces TFEB expression.

To verify the biological significance of TFEB nuclear translocation, we measured lysosomes by Lysotracker staining (28). Treatment with PNU282987 and carbachol increased Lysotracker staining compared to vehicle alone **(Fig. 3I-Q)**, which correlated with the TFEB N/C ratios of each treatment (**Fig. 3G, H**). Moreover, MG624 suppressed Lysotracker staining (**Fig. 3L, O, Q**), in correlation with the reduced TFEB expression. These data suggest that the induced nuclear TFEB is active.

Phagocytosis functions upstream of TFEB to drive its nuclear localization (62). To test if PNU282987 might activate phagocytosis as a mechanism for TFEB activation, we measured phagocytosis and bactericidal killing of *Escherichia coli* and of *Staphylococcus aureus,* which is more resistant to bactericide (63, 64). In both infection models, PNU282987 and carbachol pre-treatment had no effect on either bacterial uptake or bactericidal killing by wild type BMDMs compared to vehicle controls (**Fig. S9A, B**). Therefore, TFEB activation by PNU282987 is

unlikely a result of increased phagocytic activity and nor did PNU282987 pre-dispose macrophages to kill bacteria more efficiently.

PNU282987 might be toxic, which could activate TFEB in stressed cells. To measure toxicity of PNU282987, we treated BMDMs with PNU282987 and measured cell viability. Over a 128-fold concentration range, PNU282987 or carbachol did not cause significant cell death in wild type (**Fig. S9C, D**) and *Chrna7*$^{-/-}$ BMDMs (**Fig. S9E, F**). These results are consistent with a previous study using murine peritoneal macrophages (24) and a recent report using RAW264.7 cells (47). These data ruled out toxic stress as a mechanism of TFEB activation by PNU282987.

PNU282987 induces ROS, which are required for TFEB activation

We and others recently showed that oxidative stress and reactive oxygen species can activate TFEB in macrophages and other cell types (36, 38, 55). Therefore, PNU282987 could plausibly activate TFEB via ROS. To test if PNU282987 induces ROS production, we measured ROS levels in PNU282987-treated BMDMs. PNU282987 induced both the accumulation of ROS overall and H_2O_2 specifically (**Fig. 4A, B**). Surprisingly, MG624 suppressed ROS and H_2O_2 accumulation induced by PNU282987(**Fig. 4A, B**). MG624 alone also depressed H_2O_2 levels compared to vehicle controls, suggesting that this compound may be redox active (**Fig. 4B**). These results showed that PNU282987 induces ROS in BMDMs, which could be a mechanism for TFEB activation.

At baseline, *Chrna7*$^{-/-}$ BMDMs showed significantly higher total ROS and H_2O_2 compared to wild type cells (**Fig. 4C, D**). The ROS and H_2O_2 levels in *Chrna7*$^{-/-}$ BMDMs were similar to those in PNU282987-treated wild type BMDMs, and treatment with PNU282987 did not lead to further increases (**Fig. 4E, F**). Taken together, these results showed that PNU282987

induces ROS and MG624 inhibits them, providing a plausible hypothesis for the activation of TFEB by PNU282987 through ROS and its inhibition by MG624. To directly test this hypothesis, we attempted to disrupt TFEB nuclear localization with antioxidants NAC and NACA. However, both agents induced TFEB nuclear localization on their own, precluding this test (not shown).

TFEB activation by PNU282987 requires MCOLN1, calcineurin, and protein kinase D.

As an alternative way to test the mechanism of activation of TFEB, we examined the ROS-MCOLN1-calcineurin pathway. In previous studies, we showed that phagocytosis activates TFEB through a pathway that involves ROS, Ca^{2+} release, and calcineurin, in that sequence (38). To examine the role of intracellular Ca^{2+} in PNU282987-induced TFEB translocation, we pre-treated immortalized BMDMs expressing GFP-TFEB (38) with cell-permeable Ca^{2+}-chelating agent BAPTA-AM prior to PNU282987 treatment. BAPTA-AM pretreatment suppressed the PNU282987-induced nuclear localization of GFP-TFEB (**Fig. 5C, E**), suggesting that intracellular Ca^{2+} is required for PNU282987-induced TFEB nuclear localization. Consistently, silencing of *Trpml1*, which encodes the main lysosomal Ca^{2+} transporter MCOLN1, also prevented GFP-TFEB translocation induced by PNU282987 (**Fig. 5K-M)**, suggesting that Ca^{2+} export from the lysosome by MCOLN1 is required.

Similarly, pre-treatment with FK506, which inhibits calcineurin (65), prevented GFP-TFEB nuclear translocation caused by PNU282987 (**Fig. 5D, E**). This result suggested that calcineurin is required for PNU282987 to induce TFEB translocation. In support of this conclusion, silencing of *Ppp3cb* and *Ppp3r1*, respectively encoding catalytic and regulatory subunits of calcineurin, partially suppressed PNU282987-induced GFP-TFEB translocation (**Fig.**

5F-I, M). These results strongly suggest that calcineurin is required for PNU282987-induced TFEB activation.

In our previous research, we found that protein kinase D1 is required for TFEB activation during bacterial infection and phagocytosis (38, 66). To test whether protein kinase D might be involved in the PNU282987-induced activation of TFEB, we used the inhibitor kb-NB142-70 (67). Pretreatment of BMDMs with kb-NB142-70 suppressed TFEB translocation caused by PNU282987 (**Fig. S9G-K**), thus implicating protein kinase D in this mechanism of activation as well. Taken altogether, these results are consistent with PNU282987-induced activation of TFEB through the ROS-MCOLN1-calcineurin pathway.

TFEB mediates a large fraction of the transcriptional response to PNU282987

To define the extent to which TFEB activation drives the transcriptional response to PNU282987, we performed RNA-seq of conditionally TFEB-deleted BMDMs (38). The expression of a set of 23 macrophage differentiation markers was not significantly different between *Tfeb*$^{fl/fl}$ and *Tfeb*$^{\Delta LysM}$ BMDMs, showing that *in vitro* macrophage differentiation was not affected by *Tfeb* deletion (**Fig. S10A**).

At baseline, TFEB deletion decreased the expression of 665 genes compared to *Tfeb*$^{fl/fl}$ controls (**Fig. S10B and Table S9**). Surprisingly, this gene set was not enriched for autophagy nor lysosomal genes, as would have been expected based on data from other cell types (68). Instead, this TFEB-dependent gene set was enriched in functional categories related to “PI3K-Akt signaling”, “ECM-receptor interaction”, “Proteoglycans in cancer”, and the extracellular matrix (**Fig. S10C, Table S10**). TFEB deletion also resulted in higher expression of 138 genes (**Table S9**), but this gene set did not exhibit significant enrichment of functional categories.

These results suggest that TFEB promotes the expression of extracellular matrix genes in resting macrophages.

In PNU282987-treated cells compared to wild type, deletion of TFEB resulted in decreased expression of TNF signaling genes in addition to the baseline defect in the expression of genes related to extracellular matrix and PI3K-AKT (**Fig. 6A, B**). The genes that were more highly expressed in TFEB-deleted cells were not significantly enriched for any informative functional category. Thus, TFEB promotes the expression of TNF signaling genes in response to PNU282987.

Of 118 genes that were upregulated by PNU282987 in wild type controls, only 66 were also upregulated in TFEB-deleted BMDMs (**Fig. 6C**). 19 additional genes were induced only in TFEB-deleted cells. None of these gene sets, *i.e.* TFEB-dependent, -independent, or compensatory, were enriched for any relevant functional category. Thus, TFEB is required for about 40% of the transcriptional response that is triggered in wild type BMDMs by PNU282987.

From these analyses, gene *Tnfsf15* stood out as the sole PNU282987-induced gene encoding a soluble signaling mediator. Tumor necrosis factor superfamily-15 (TNFSF15), also called TL1A, is a ligand for death receptor 3 (DR3), which activates signaling pathways involved in the activation, proliferation, apoptosis, and pro-inflammatory responses in immune cells, including monocytes and macrophages (69). Therefore, it was possible that PNU282987 induced TNFSF15 production as well as its transcription, leading to an activated macrophage state *in vitro*. To test that hypothesis, we performed ELISA using supernatants from wild type and *Tfeb*$^{fl/fl}$ BMDMs. Treatment with PNU282987 did not increase soluble TNFSF15 in these cells

(**Fig. S10D**), suggesting that TNFSF15 is not likely to be a mediator of PNU282987-induced pro-inflammatory gene expression.

To further test these conclusions, we turned to RAW264.7 cells that were deleted for *Tfeb* and *Tfe3,* which encodes a TFEB paralog that heterodimerizes with TFEB but can also function independently as a homodimer (39, 70). In this system, PNU282987-treated *Tfeb Tfe3* double knockout cells showed defective expression of 550 genes compared to wild type controls (**Fig. S11A, Table S11**). These genes were enriched in pro-inflammatory pathways, notably TNF and NOD receptor signaling, as well as lysosomal genes (**Fig. S11B, Table S12**), showing that TFEB and TFE3 are important for the pro-inflammatory gene expression program that is triggered by PNU282987. The genes that were more highly expressed in the *Tfeb Tfe3* knockout cells did not show enrichment of any relevant functional categories. These data strongly support the conclusion that PNU282987 induces a pro-inflammatory gene expression signature in a TFEB and TFE3-dependent manner.

Recall that PNU282987 did not induce cytokine secretion in RAW264.7 cells, despite their transcriptional induction (**Fig. S11C-F**). Surprisingly, deletion of *Tfeb* and *Tfe3* completely abrogated IL-6 and IFN-β1 production by LPS (but not that of TNF-α, **Fig. S11C-F**). Moreover, PNU282987 induced a 3-fold increase in LDH release in the *Tfeb Tfe3* knockout cells (**Fig. S11G**), suggesting that TFEB and TFE3 may mitigate PNU282987 cellular toxicity.

However, at baseline *Tfeb Tfe3* double knockout RAW264.7 cells showed decreased genes expression of macrophage differentiation markers CD11b, CD15, CD16, CD32, CD64, CD33, and CD86, as well as TLR2 and TLR4 compared to wild type (**Fig. S11H, Table S13**), suggesting that the *Tfeb Tfe3* double knockout RAW264.7 cells may show an impaired

macrophage phenotype compared to the wild type control. As with the wild type RAW264.7 cells, the double knockout cells did not detectably express cholinergic receptors, except α10NAChR, for which the transcript was detected at the same level as in wild type cells (**Fig. S11I**). *Tfeb*$^{fl/fl}$ and *Tfeb*$^{\Delta LysM}$ BMDMs did not show expression of any cholinergic receptor, similar to wild type BMDMs (**Fig. 2C, S11I**). Taken together, these data show that TFEB (and TFE3) are important mediators of the PNU282987-induced pro-inflammatory gene transcription response in macrophages.

DISCUSSION

We describe the early phenotypic effects of PNU282987 treatment on macrophage gene expression *in vitro*. PNU282987 triggered a large number of pro-inflammatory genes in naïve primary macrophages and macrophage cell lines. We show evidence that these pro-inflammatory expression profiles do not result in increased cytokine secretion, at least at the exposure times that we examined. Because we did not find conclusive evidence of cholinergic receptor expression in primary macrophages of diverse genetic backgrounds nor in the RAW264.7 cell line, we hypothesize that PNU282987 may instead exert this activity by cellular stress. Consistent with this hypothesis, we observe TFEB activation in PNU282987-treated cells, and deletion of TFEB (and TFE3) significantly impaired PNU282987-induced gene expression changes. Furthermore, we provide evidence that PNU282987induces the accumulation of ROS in treated macrophages, and that they trigger TFEB activation through the previously described ROS-MCOLN1-calcineurin Ca^{2+} signaling pathway. Thus, our findings reveal at least three key insights.

The first key insight is that secreted pro-inflammatory cytokines (e.g. IFN-β1, IL-6 and TNF-α) did not increase following PNU282987 treatment, despite their gene induction. It is

507 possible that longer exposure times (>12 h) might result in induced release. However, we
508 focused on primary effects of PNU282987 treatment as opposed to the effects of long-term
509 exposure to avoid confounding secondary responses. Alternatively, the cytokines may be
510 regulated post-transcriptionally. This interpretation has precedent: transcription of inflammatory
511 mediators such as TNF-α and IL-6 is uncoupled from secretion by post-transcriptional regulation
512 mechanisms at the level of mRNA stability or mRNA translation (71). Our RNA-seq analysis
513 showed induction of *Zfp36l1* in wild type and *Tfeb*$^{fl/fl}$ BMDMs by PNU282987. *Zfp36l1* encodes
514 RNA-binding protein Tristetraprolin (TTP), which belongs to the ZFP36 family of proteins
515 involved in post-transcriptional regulation of many inflammatory genes (72, 73). Whether
516 *Zfp36l1* contributes to uncoupling TNF-α or IL-6 gene expression from secretion under these
517 conditions requires further investigation. Consistently, a 5 min pre-treatment with ACh was
518 sufficient to repress LPS-induced TNF-α, IL-1β, and IL-6 secretion in human monocyte-derived
519 macrophages, without significant effects on their transcripts (1). Therefore, it is likely that
520 PNU282987-induced cytokine transcription does not result in enhanced secretion due to post-
521 transcriptional regulation.

522 The induction of pro-inflammatory gene expression by PNU282987 appears to run
523 contrary to the large body of data supporting a cholinergic anti-inflammatory pathway (CAIP).
524 Studies show that stimulation with ACh or α7NAChR agonists, such as nicotine or choline,
525 dampen inflammation by suppressing NF-κB in LPS-stimulated human monocyte-derived
526 macrophages or RAW264.7 macrophages (9, 74). PNU282987 treatment alleviated diverse
527 inflammatory conditions in mice, such as sepsis-associated lung injury (25), psoriasis-like
528 inflammation (51), or experimental colitis (27) by inhibiting NF- κB. A unifying theme in these
529 studies is that PNU282987 was administered to already activated macrophages. Because we were

530 interested in the primary effects in naïve macrophages, this represents a significant difference
531 with our approach. Nonetheless, we replicate the inhibitory effect of PNU29287 on LPS-induced
532 secretion of TNF-α and IL-6. However, the lack of detectable α7NAChR expression in our
533 systems casts doubt on an α7NAChR-mediated mechanism of action. Published work implicated
534 JAK2 in the mechanism of cholinergic anti-inflammatory effects through NF-κB repression (7,
535 75); yet other reports showed that JAK2 can be activated by ROS (76, 77), supporting an
536 alternative explanation. Moreover, nicotine triggers ROS in murine BMDMs (78) and
537 RAW264.7 macrophages (79), lending further support to a ROS-mediated mechanism.

538 The second key insight is the surprising lack of cholinergic receptor expression by
539 macrophages. Early reports measured the expression of α7NAChR in primary human
540 macrophages using a nested RT-PCR technique and western blot with α7NAChR antibody
541 specific to rat and human α7 subunit (3) and in mouse alveolar macrophages using
542 immunofluorescence (80). However, these studies did not show the specificity of the antibodies
543 with *Chrna7*$^{-/-}$ controls. Another study reported α7NAChR expression in IFN-γ-polarized and IL-
544 4-polarized BMDMs using RT-PCR (not RT-qPCR), but naïve macrophages were not tested (81).
545 In yet another study, α7NAChR mRNA expression by RT-PCR was reported in thioglycolate-
546 elicited peritoneal macrophages that were stimulated with LPS for 24 h (48), or in murine bone
547 marrow cells, with high variability among littermates (82). Undetectable or highly variable
548 expression of *Chrna7* transcript among mononuclear phagocytes, as well as levels of *Chrna7*
549 mRNA not correlating with expression of functional receptors have been noted (83). Large-scale
550 studies, including our own RNA-seq experiments, do not detect *Chrna7* expression either in
551 BMDMs or various tissue-resident macrophages, even after pro-inflammatory activation (84). In
552 our hands, the same oligonucleotide primers that were reported (47, 48, 85) were unable to detect

553 *Chrna7* transcript by highly sensitive RT-qPCR (**Table S14**). Thus, we are unable to conclude
554 that murine naïve bone marrow-derived macrophages express *Chrna7* transcript.

555 In addition, we used α-bungarotoxin to detect surface expression of α7NAChR by flow
556 cytometry, similar to previous studies that detected α7NAChR expression on murine intestinal
557 muscularis macrophages (53) and human primary macrophages (54) but were not able to detect
558 α7NAChR protein expression in murine peritoneal or muscularis macrophages. The Human
559 Protein Atlas and ImmGen databases do not support α7NAChR expression in macrophages of
560 various origins (**Fig. S7, S8**). Thus, there is a lack of unequivocal evidence of α7NAChR
561 expression in macrophages.

562 It is possible that specific stimuli induce α7nAChR expression. α7NAChR expression by
563 RT-qPCR was reported to increase in human monocyte-derived macrophages following
564 treatment with apolipoproteins (86). However, α7NAChR expression was undetectable in
565 untreated controls, by RT-qPCR, fluorescence staining, and immunoblot. Using the same
566 antibody, we also failed to detect α7NAChR expression in naïve BMDMs. Another study
567 reported α7NAChR expression in J774A.1 cells and murine peritoneal macrophages following
568 LPS treatment but reported no expression in unstimulated macrophages by FITC-labelled
569 bungarotoxin fluorescence imaging and immunoblot (87). In contrast, a recent study reported no
570 differences in *Chrna7* mRNA expression of α7nAChR between LPS treated and untreated
571 RAW264.7 macrophages by RT-qPCR , but the levels of expression were very low (47). We were
572 unable to detect expression after testing the same primer pairs. Additionally, we found no α-
573 bungarotoxin staining in murine colonic macrophages from *Salmonella enterica*-infected animals
574 (**Fig. S6A, B**). Thus, it is unclear whether LPS or other stimuli induce *Chrna7* in murine
575 macrophages.

576 *Chrna7*$^{-/-}$ macrophages were severely impaired in their response to PNU282986. These
577 results are difficult to reconcile with the lack of α7NAChR expression. One possibility is that the
578 whole-animal deletion might impair the bone marrow compartment and affect *in vitro* properties
579 (but not differentiation *per se*, see **Fig. S2C**) of BMDMs. To address this possibility, we
580 attempted a conditional deletion strategy to delete *Chrna7* in monocytes (88) but were
581 unsuccessful in generating the strain. Alternatively, genetic background may affect the behavior
582 of the knockout cells. The *Chrna7* knockout was constructed by deleting *Chrna7* exons 8-10 in
583 the 129/SvEv background and introduced in the C57BL/6 background (49). It is possible that
584 genomic elements surrounding the transgene or retention of 129S genome affect BMDM
585 responses to chemical probes such as PNU282987 (89). Whichever the case, we cannot exclude a
586 contribution of the *Chrna7* locus to the macrophage response to PNU282987 despite its lack of
587 expression. For instance, our data show that the *Chrna7* knockout cells exhibit a constitutively
588 higher level of ROS than wild type, which may desensitize them to PNU282987 through
589 mechanisms that do not hinge on *Chrna7* expression.

590 Given the lack of conclusive evidence showing cholinergic receptor expression, it is
591 surprising that MG624 inhibited the nuclear translocation of TFEB and lysosomal biogenesis by
592 PNU29287. We observed decreased staining of TFEB in MG624-treated cells, suggesting that
593 MG624 independently causes TFEB repression, which could explain its suppression of
594 lysosomal biogenesis caused by PNU282987. It is unclear if this mechanism of TFEB repression
595 is transcriptional or post-transcriptional.

596 Another key insight is that TFEB was both activated by PNU282987 and biologically
597 significant for the transcriptional response to it. TFEB was shown to be activated by PNU282987
598 in murine neuronal N2a cells (90) and in pancreatic acinar cells (91), suggesting that this activity

599 of PNU282987 may extend beyond macrophages. We find that the mechanism of TFEB
600 activation in macrophages involves the ROS-responsive MCOLN1-Ca^{2+}-calcineurin pathway
601 that we described previously (38). Additional upstream regulators of TFEB, such as mTORC1
602 (92), PKC-α (66) and PKC-β (93), LRRK2 (94), ERK2 (29), p38 MAPK(95), and AKT (96)
603 could also be involved, but further investigation is required to assess their relevance in the
604 context of PNU282987-induced TFEB activation.

605 *Tfeb Tfe3* dKO RAW264.7 cells exhibited a stronger defect than *Tfeb*$^{\Delta Lysm}$ BMDMs,
606 which could be due to the partial redundancy between TFEB and TFE3. We also detected
607 defective expression of several macrophage markers in the *Tfeb Tfe3* dKO RAW264.7 cells;
608 nonetheless, these cells remain capable of secreting LPS-induced TNF-α (**Fig. S11D**), and of
609 phagocytosis and bactericidal killing (38), ruling out a dramatic defect in macrophage
610 differentiation. However, this may also reflect biological differences between primary cells and
611 the cell line. Previous work suggested that TFEB was required for human THP-1 cell
612 differentiation induced by PMA (97); in contrast, we did not detect a defect in BMDM
613 differentiation in *Tfeb*-deleted murine cells. Furthermore, we previously showed that PMA
614 activates TFEB *via* protein kinase D1 (66). Thus, PMA may activate a TFEB-dependent
615 differentiation path in THP-1 cells that is not fully representative of *in vivo* differentiation or M-
616 CSF-driven *in vitro* differentiation, as in our model system.

617 The mechanism of PNU282987-induced ROS is currently unknown. Cellular sources of
618 endogenous ROS include mitochondria, but how PNU282987 affects mitochondrial function in
619 macrophages is not known. Moreover, the mechanism by which MG624 reduces TFEB
620 expression is also unknown. TFEB is degraded by ubiquitination and the proteasome in HeLa
621 cells (98) and neuron-like SH-SY5Y cells or HEK293 cells (99), but whether MG624 affects

622 TFEB ubiquitination or proteasomal degradation is unknown. Nonetheless, our findings provide
623 new insight into the mechanisms of action of two widely used chemical agents that are broadly
624 believed to be highly specific and shed new light on the central role of TFEB in the regulation of
625 transcriptional phenotypes in macrophages. Based on our results, the interpretation of
626 experiments that use PNU29287, carbachol, MG624, and potentially other cholinergic agents,
627 must take into account this alternative mechanism of action.

628 **FIGURE LEGENDS**

629 **Figure 1. PNU282987 induces pro-inflammatory genes in BMDMs**

630 **A**. RNA-seq of BMDMs treated with PNU282987 (50 μM, 2 h) or DMSO. Volcano plot of
631 differentially expressed genes in PNU282987 treated cells relative to DMSO treated control (fold
632 change (FC) ≥ 1.5; Padj. ≤ 0.01). Red indicates upregulated (UP), blue denotes downregulated
633 (DOWN) genes.

634 **B.** Gene ontology (GO) over-representation and KEGG pathway enrichment analysis of
635 PNU282987 induced genes.

636 **C-G.** Measurement of secreted cytokines by ELISA from wild type (WT) BMDMs under the
637 following conditions: untreated (unt), DMSO, PNU282987 (50 μM, 12 h), LPS (100 ng/mL, 12
638 h), LPS (100 ng/mL, 2 h) + PNU282987 (50 μM, 12 h), PNU282987 (50 μM, 2 h) + LPS (100
639 ng/mL, 12 h). Cytokines: IL-6 (**C**), TNF-α (**D**), IFN-β1 (**E**), IL-1β (**F**), and IL-10 (**G**).

640 **H.** Lactate dehydrogenase (LDH) release measured in culture supernatants.

641 n = 3 biological replicates, *p ≤ 0.05, **p ≤ 0.01, ***p ≤ 0.001, ****p ≤ 0.0001, One-way
642 ANOVA followed by Tukey's post-hoc test.

Figure 2. BMDMs from *Chrna7*$^{-/-}$ mice are defective in the transcriptional response to PNU282987

A. RT-qPCR, relative expression of *Chrna7*, *Chnrb2,* and *Il6* normalized to *Gapdh,* of mouse whole brain lysate following PBS or LPS (2 mg/kg, 24 h) intraperitoneal injections (3 biological replicates).

B. RT-qPCR of *Chrna7* in WT and *Chrna7*$^{-/-}$ BMDMs relative to *Gapdh* (4 biological replicates, ns: not significant ($p \geq 0.05$, 2-sample 2-sided unpaired *t* test).

C. RT-qPCR of transcripts encoding various nicotinic and muscarinic receptor subunit genes in WT and *Chrna7*$^{-/-}$ BMDMs (4 biological replicates, Two-way ANOVA, multiple comparisons, ****$p \leq 0.0001$)

D. Venn diagram showing the overlap between PNU282987-induced genes in WT BMDMs compared to PNU282987-induced genes in *Chrna7*$^{-/-}$ BMDMs.

E. Volcano plot showing differentially expressed genes in PNU282987-treated *Chrna7*$^{-/-}$ BMDMs compared to wild type. Red, upregulated genes in PNU282987 treated *Chrna7*$^{-/-}$ BMDMs; blue, upregulated genes in PNU282987 wild type BMDMs (fold change (FC) ≥ 1.5; Padj. ≤ 0.01).

F. GO over-representation and KEGG pathway analysis for genes upregulated in PNU282987-treated WT BMDMs.

663 **Figure 3. PNU282987 activates TFEB in BMDMs**

664 **A-F.** Representative immunofluorescence micrographs of WT BMDMs stained with anti-TFEB
665 antibody, treated with DMSO control (**A**), PNU282987 (50 μM, 2 h) (**B**), MG624 (1 μM, 2 h)
666 (**C**), MG624 (1 μM, 2 h pre-treatment) + PNU282987 (50 μM, 2 h) (**D**), Carbachol (50 μM, 2 h)
667 (**E**), MG624 (1 μM, 2 h pre-treatment) + Carbachol (50 μM, 2 h) (**F**).

668 **G, H.** Nucleus to cytoplasmic (N:C) ratio of TFEB in BMDMs, measured using CellProfiler
669 software (400 cells per condition, **$p \leq 0.01$, ****$p \leq 0.0001$, One-way ANOVA followed by
670 Tukey's post-hoc test).

671 **I-P.** LysoTracker staining (red) of GFP-TFEB iBMDMs treated with DMSO control (**I**),
672 PNU282987 (50 μM, 2 h) (**J**), Carbachol (50 μM, 2 h) (**M**) or MG624 (1 μM, 2 h) (**K**) MG624
673 (1 μM, 2 h pre-treatment) + PNU282987 (50 μM, 2 h) (**L**), MG624 (1 μM, 2 h pre-treatment) +
674 Carbachol (50 μM, 2 h) (**O**) with LPS (100 ng/mL, 2 h) (**N**) and Torin-1 (1.25 uM, 1 h) (**P**).

675 (**Q**) LysoTracker mean fluorescence intensity per cell (MFI/cell) measured with CellProfiler.
676 Images and quantification of 3 biological replicates (400 cells per condition, ****$p \leq 0.0001$,
677 One-way ANOVA followed by Tukey's post-hoc test).

678 **Figure 4. PNU282987 induces ROS production**

679 **A, B.** Total ROS (**A**) and (**B**) superoxide in WT BMDMs treated with DMSO, PNU282987 (50
680 μM, 2 h), or following pre-treatment with MG624 (1 μM, 2 h). Pyocyanin (200 μM, 30 min) and
681 NAC (5 mM, 30 min), positive and negative control, respectively. (400 cells per condition, *$p \leq$
682 0.05, ****$p \leq 0.0001$, One-way ANOVA followed by Tukey's post-hoc test).

683 **C, D.** Total ROS (**C**) and superoxide (**D**) shown as mean fluorescence intensity in WT and
684 *Chrna7*$^{-/-}$ BMDMs (200 cells per condition, ***$p \leq 0.0001$, 2-sided 2-sample unpaired *t* test).

685 **E, F.** Total ROS (**E**) and superoxide (**F**) measured in WT and *Chrna7*$^{-/-}$ BMDMs following
686 treatment with PNU282987 (50 μM, 2 h), NAC (5 mM, 30 min) and Pyocyanin (200 μM, 30
687 min). 400 cells per condition, ****$p \leq 0.0001$, One-way ANOVA followed by Tukey's post-hoc
688 test.

689 **Figure 5. TFEB activation by PNU282987 requires MCOLN1 and calcineurin**

690 **A-D.** Representative fluorescence micrographs of GFP-TFEB iBMDMs treated with DMSO (**A**),
691 PNU282987 (50 μM, 2 h) (**B**), and PNU282987 (50 μM, 2 h) following pre-treatment with
692 BAPTA-AM (10 μM, 3 h) (**C**) or FK506 (5 μM, 6 h) (**D**).

693 **E.** Quantification of TFEB N:C ratio using CellProfiler (3 biological replicates, 350 cells per
694 condition, ****$p \leq 0.0001$, One-way ANOVA followed by Tukey's post-hoc test).

695 **F-L.** Representative fluorescence micrographs of GFP-TFEB iBMDMs treated with siRNA,
696 scrambled (*Scr*) (**F, G**) or directed against *Ppp3cb* (**H**), *Ppp3r1* (**I**), and *Trpml1* (**K, L**) for 48 h
697 prior to treatment with PNU282987 (50 μM, 2 h) or serum starvation (**J, L**).

698 **M.** Quantification of GFP-TFEB N:C ratio by CellProfiler (3 biological replicates, n=300 cells)
699 **** $p \leq 0.0001$ (one-way ANOVA followed by Tukey's post-hoc test).

700 **Figure 6. TFEB mediates 40% of the transcriptional response to PNU282987 in BMDMs**

701 **A.** Volcano plot showing differentially expressed genes in PNU282987-induced *Tfeb*$^{\Delta LysM}$
702 BMDMs compared to PNU282987-induced *Tfeb*$^{fl/fl}$ BMDMs. Red, upregulated genes in
703 PNU282987-treated *Tfeb*$^{\Delta LysM}$ BMDMs and blue, upregulated genes in PNU282987-treated
704 *Tfeb*$^{fl/fl}$ BMDMs (fold change (FC) ≥ 1.5; Padj. ≤ 0.01).

705 **B.** Gene ontology (GO) over-representation and (KEGG) pathway enrichment analysis of
706 PNU282987 induced genes in *Tfeb*$^{fl/fl}$ BMDMs.

707 **C.** Venn diagram showing the overlap between PNU282987-induced genes in *Tfeb*$^{fl/fl}$ BMDMs
708 and PNU282987-induced genes in *Tfeb*$^{\Delta LysM}$ BMDMs.

709 **REFERENCES**

710 1. Borovikova LV, Ivanova S, Zhang M, Yang H, Botchkina GI, Watkins LR, et al. Vagus
711 nerve stimulation attenuates the systemic inflammatory response to endotoxin. Nature.
712 2000;405(6785):458-62.
713 2. Kelly MJ, Breathnach C, Tracey KJ, Donnelly SC. Manipulation of the inflammatory
714 reflex as a therapeutic strategy. Cell Reports Medicine. 2022;3(7).
715 3. Wang H, Yu M, Ochani M, Amella CA, Tanovic M, Susarla S, et al. Nicotinic
716 acetylcholine receptor α7 subunit is an essential regulator of inflammation. Nature.
717 2003;421(6921):384-8.
718 4. Rosas-Ballina M, Olofsson PS, Ochani M, Valdés-Ferrer SI, Levine YA, Reardon C, et al.
719 Acetylcholine-synthesizing T cells relay neural signals in a vagus nerve circuit. Science.
720 2011;334(6052):98-101.
721 5. Baez-Pagan CA, Delgado-Velez M, Lasalde-Dominicci JA. Activation of the Macrophage
722 alpha7 Nicotinic Acetylcholine Receptor and Control of Inflammation. J Neuroimmune
723 Pharmacol. 2015;10(3):468-76.
724 6. Yoshikawa H, Kurokawa M, Ozaki N, Nara K, Atou K, Takada E, et al. Nicotine inhibits
725 the production of proinflammatory mediators in human monocytes by suppression of I-κB
726 phosphorylation and nuclear factor-κB transcriptional activity through nicotinic acetylcholine
727 receptor α7. Clinical & Experimental Immunology. 2006;146(1):116-23.

728 7. de Jonge WJ, van der Zanden EP, The FO, Bijlsma MF, van Westerloo DJ, Bennink RJ, et
729 al. Stimulation of the vagus nerve attenuates macrophage activation by activating the Jak2-
730 STAT3 signaling pathway. Nat Immunol. 2005;6(8):844-51.
731 8. Van Westerloo DJ, Giebelen IA, Florquin S, Daalhuisen J, Bruno MJ, de Vos AF, et al.
732 The cholinergic anti-inflammatory pathway regulates the host response during septic peritonitis.
733 Journal of Infectious Diseases. 2005;191(12):2138-48.
734 9. Wang H, Liao H, Ochani M, Justiniani M, Lin X, Yang L, et al. Cholinergic agonists
735 inhibit HMGB1 release and improve survival in experimental sepsis. Nature medicine.
736 2004;10(11):1216-21.
737 10. Ghia JE, Blennerhassett P, Kumar–Ondiveeran H, Verdu EF, Collins SM. The vagus
738 nerve: a tonic inhibitory influence associated with inflammatory bowel disease in a murine
739 model. Gastroenterology. 2006;131(4):1122-30.
740 11. Bai A, Guo Y, Lu N. The effect of the cholinergic anti-inflammatory pathway on
741 experimental colitis. Scandinavian journal of immunology. 2007;66(5):538-45.
742 12. Westman M, Engström M, Catrina A, Lampa J. Cell specific synovial expression of
743 nicotinic alpha 7 acetylcholine receptor in rheumatoid arthritis and psoriatic arthritis.
744 Scandinavian journal of immunology. 2009;70(2):136-40.
745 13. van Maanen MA, Lebre MC, van der Poll T, LaRosa GJ, Elbaum D, Vervoordeldonk MJ,
746 et al. Stimulation of nicotinic acetylcholine receptors attenuates collagen-induced arthritis in
747 mice. Arthritis & Rheumatism. 2009;60(1):114-22.
748 14. Gwilt CR, Donnelly LE, Rogers DF. The non-neuronal cholinergic system in the airways:
749 an unappreciated regulatory role in pulmonary inflammation? Pharmacology & therapeutics.
750 2007;115(2):208-22.

751 15. Su X, Matthay MA, Malik AB. Requisite role of the cholinergic α7 nicotinic
752 acetylcholine receptor pathway in suppressing gram-negative sepsis-induced acute lung
753 inflammatory injury. The journal of immunology. 2010;184(1):401-10.
754 16. Greene CM, Ramsay H, Wells RJ, O'Neill SJ, McElvaney NG. Inhibition of Toll-Like
755 Receptor 2-Mediated Interleukin-8 Production in Cystic Fibrosis Airway Epithelial Cells via the
756 α7-Nicotinic Acetylcholine Receptor. Mediators of Inflammation. 2010;2010.
757 17. Marrero MB, Lucas R, Salet C, Hauser TA, Mazurov A, Lippiello PM, et al. An α7
758 nicotinic acetylcholine receptor-selective agonist reduces weight gain and metabolic changes in a
759 mouse model of diabetes. Journal of Pharmacology and Experimental Therapeutics.
760 2010;332(1):173-80.
761 18. Pavlov VA, Tracey KJ. The vagus nerve and the inflammatory reflex—linking immunity
762 and metabolism. Nature Reviews Endocrinology. 2012;8(12):743-54.
763 19. Bencherif M, Lippiello PM, Lucas R, Marrero MB. Alpha7 nicotinic receptors as novel
764 therapeutic targets for inflammation-based diseases. Cell Mol Life Sci. 2011;68(6):931-49.
765 20. Youssef ME, Moustafa Y, Abdelrazek H. Molecular mechanisms of α7-nAchR-mediated
766 anti-inflammatory effects. Indian Journal of Physiology and Pharmacology. 2021;64(3):158-73.
767 21. Lu B, Kwan K, Levine YA, Olofsson PS, Yang H, Li J, et al. α7 nicotinic acetylcholine
768 receptor signaling inhibits inflammasome activation by preventing mitochondrial DNA release.
769 Molecular medicine. 2014;20:350-8.
770 22. Bodnar AL, Cortes-Burgos LA, Cook KK, Dinh DM, Groppi VE, Hajos M, et al.
771 Discovery and structure− activity relationship of quinuclidine benzamides as agonists of α7
772 nicotinic acetylcholine receptors. Journal of medicinal chemistry. 2005;48(4):905-8.

773 23. Hajos M, Hurst R, Hoffmann W, Krause M, Wall T, Higdon N, et al. The selective α7
774 nicotinic acetylcholine receptor agonist PNU-282987 [N-[(3R)-1-azabicyclo [2.2. 2] oct-3-yl]-4-
775 chlorobenzamide hydrochloride] enhances GABAergic synaptic activity in brain slices and
776 restores auditory gating deficits in anesthetized rats. Journal of Pharmacology and Experimental
777 Therapeutics. 2005;312(3):1213-22.
778 24. Shao Z, Li Q, Wang S, Chen Z. Protective effects of PNU-282987 on sepsis-induced
779 acute lung injury in mice. Molecular Medicine Reports. 2019;19(5):3791-8.
780 25. Pinheiro NM, Santana FPR, Almeida RR, Guerreiro M, Martins MA, Caperuto LC, et al.
781 Acute lung injury is reduced by the α7nAChR agonist PNU-282987 through changes in the
782 macrophage profile. The FASEB Journal. 2017;31(1):320-32.
783 26. Zhao X, Yu Z, Lv Z, Meng L, Xu J, Yuan S, et al. Activation of alpha-7 nicotinic
784 acetylcholine receptors (α7nAchR) promotes the protective autophagy in LPS-induced acute
785 lung injury (ALI) in vitro and in vivo. Inflammation. 2019;42:2236-45.
786 27. Pu W, Su Z, Wazir J, Zhao C, Wei L, Wang R, et al. Protective effect of α7 nicotinic
787 acetylcholine receptor activation on experimental colitis and its mechanism. Molecular
788 Medicine. 2022;28(1):104.
789 28. Sardiello M, Palmieri M, Di Ronza A, Medina DL, Valenza M, Gennarino VA, et al. A
790 gene network regulating lysosomal biogenesis and function. Science. 2009;325(5939):473-7.
791 29. Settembre C, Di Malta C, Polito VA, Arencibia MG, Vetrini F, Erdin S, et al. TFEB links
792 autophagy to lysosomal biogenesis. science. 2011;332(6036):1429-33.
793 30. Martina JA, Diab HI, Brady OA, Puertollano R. TFEB and TFE 3 are novel components
794 of the integrated stress response. The EMBO journal. 2016;35(5):479-95.

795 31. Nabar NR, Kehrl JH. Focus: Infectious Diseases: The Transcription Factor EB Links
796 Cellular Stress to the Immune Response. The Yale Journal of Biology and Medicine.
797 2017;90(2):301.
798 32. Roczniak-Ferguson A, Petit CS, Froehlich F, Qian S, Ky J, Angarola B, et al. The
799 transcription factor TFEB links mTORC1 signaling to transcriptional control of lysosome
800 homeostasis. Science signaling. 2012;5(228):ra42-ra.
801 33. Settembre C, Zoncu R, Medina DL, Vetrini F, Erdin S, Erdin S, et al. A lysosome-to-
802 nucleus signalling mechanism senses and regulates the lysosome via mTOR and TFEB. The
803 EMBO journal. 2012;31(5):1095-108.
804 34. Nezich CL, Wang C, Fogel AI, Youle RJ. MiT/TFE transcription factors are activated
805 during mitophagy downstream of Parkin and Atg5. Journal of Cell Biology. 2015;210(3):435-50.
806 35. Visvikis O, Ihuegbu N, Labed SA, Luhachack LG, Alves A-MF, Wollenberg AC, et al.
807 Innate host defense requires TFEB-mediated transcription of cytoprotective and antimicrobial
808 genes. Immunity. 2014;40(6):896-909.
809 36. Zhang X, Cheng X, Yu L, Yang J, Calvo R, Patnaik S, et al. MCOLN1 is a ROS sensor in
810 lysosomes that regulates autophagy. Nature communications. 2016;7(1):12109.
811 37. Tan A, Prasad R, Lee C, Jho E-h. Past, present, and future perspectives of transcription
812 factor EB (TFEB): mechanisms of regulation and association with disease. Cell Death &
813 Differentiation. 2022;29(8):1433-49.
814 38. Najibi M, Honwad HH, Moreau JA, Becker SM, Irazoqui JE. A novel Nox/Phox-Cd38-
815 Naadp-Tfeb axis important for macrophage activation during bacterial phagocytosis. Autophagy.
816 2022;18(1):124-41.

817 39. Pastore N, Brady OA, Diab HI, Martina JA, Sun L, Huynh T, et al. TFEB and TFE3
818 cooperate in the regulation of the innate immune response in activated macrophages. Autophagy.
819 2016;12(8):1240-58.
820 40. McQuin C, Goodman A, Chernyshev V, Kamentsky L, Cimini BA, Karhohs KW, et al.
821 CellProfiler 3.0: Next-generation image processing for biology. PLoS biology.
822 2018;16(7):e2005970.
823 41. Yukselen O, Turkyilmaz O, Ozturk AR, Garber M, Kucukural A. DolphinNext: a
824 distributed data processing platform for high throughput genomics. BMC genomics. 2020;21:1-
825 16.
826 42. Reimand J, Arak T, Adler P, Kolberg L, Reisberg S, Peterson H, et al. g: Profiler—a web
827 server for functional interpretation of gene lists (2016 update). Nucleic acids research.
828 2016;44(W1):W83-W9.
829 43. Evangelista JE, Xie Z, Marino GB, Nguyen N, Clarke Daniel JB, Ma'ayan A. Enrichr-
830 KG: bridging enrichment analysis across multiple libraries. Nucleic Acids Research.
831 2023;51(W1):W168-W79.
832 44. Hulsen T. DeepVenn--a web application for the creation of area-proportional Venn
833 diagrams using the deep learning framework Tensorflow. js. arXiv preprint arXiv:221004597.
834 2022.
835 45. Koscsó B, Gowda K, Schell TD, Bogunovic M. Purification of dendritic cell and
836 macrophage subsets from the normal mouse small intestine. Journal of immunological methods.
837 2015;421:1-13.

838 46. Koscsó B, Bogunovic M. Analysis and purification of mouse intestinal dendritic cell and
839 macrophage subsets by flow cytometry. Current Protocols in Immunology. 2016;114(1):14.39. 1-
840 14.39. 14.
841 47. Tan Y, Chu Z, Shan H, Zhangsun D, Zhu X, Luo S. Inflammation regulation via an
842 agonist and antagonists of α7 nicotinic acetylcholine receptors in RAW264. 7 macrophages.
843 Marine Drugs. 2022;20(3):200.
844 48. Kawashima K, Yoshikawa K, Fujii YX, Moriwaki Y, Misawa H. Expression and function
845 of genes encoding cholinergic components in murine immune cells. Life sciences. 2007;80(24-
846 25):2314-9.
847 49. Orr-Urtreger A, Göldner FM, Saeki M, Lorenzo I, Goldberg L, De Biasi M, et al. Mice
848 deficient in the α7 neuronal nicotinic acetylcholine receptor lack α-bungarotoxin binding sites
849 and hippocampal fast nicotinic currents. Journal of Neuroscience. 1997;17(23):9165-71.
850 50. Lei W, Zhao C, Sun J, Jin Y, Duan Z. Activation of α7nAChR preserves intestinal barrier
851 integrity by enhancing the HO-1/STAT3 signaling to inhibit NF-κB activation in mice.
852 Biomedicine & Pharmacotherapy. 2022;149:112733.
853 51. Chen Y, Lian P, Peng Z, Wazir J, Ma C, Wei L, et al. Alpha-7 nicotinic acetylcholine
854 receptor agonist alleviates psoriasis-like inflammation through inhibition of the STAT3 and NF-
855 κB signaling pathway. Cell Death Discovery. 2022;8(1):141.
856 52. Nemethova A, Michel K, Gomez-Pinilla PJ, Boeckxstaens GE, Schemann M. Nicotine
857 attenuates activation of tissue resident macrophages in the mouse stomach through the β2
858 nicotinic acetylcholine receptor. PLoS One. 2013;8(11):e79264.

859 53. Matteoli G, Gomez-Pinilla PJ, Nemethova A, Di Giovangiulio M, Cailotto C, van Bree
860 SH, et al. A distinct vagal anti-inflammatory pathway modulates intestinal muscularis resident
861 macrophages independent of the spleen. Gut. 2014;63(6):938-48.
862 54. Siniavin AE, Streltsova MA, Kudryavtsev DS, Shelukhina IV, Utkin YN, Tsetlin VI.
863 Activation of α7 nicotinic acetylcholine receptor upregulates HLA-DR and macrophage
864 receptors: Potential role in adaptive immunity and in preventing immunosuppression.
865 Biomolecules. 2020;10(4):507.
866 55. Martina JA, Puertollano R. Protein phosphatase 2A stimulates activation of TFEB and
867 TFE3 transcription factors in response to oxidative stress. Journal of Biological Chemistry.
868 2018;293(32):12525-34.
869 56. Martina JA, Guerrero-Gómez D, Gómez-Orte E, Antonio Barcena J, Cabello J, Miranda-
870 Vizuete A, et al. A conserved cysteine-based redox mechanism sustains TFEB/HLH-30 activity
871 under persistent stress. The EMBO Journal. 2021;40(3):e105793.
872 57. Gotti C, Balestra B, Moretti M, Rovati G, Maggi L, Rossoni G, et al. 4-Oxystilbene
873 compounds are selective ligands for neuronal nicotinic αBungarotoxin receptors. British journal
874 of pharmacology. 1998;124(6):1197-206.
875 58. Tanibuchi Y, Wu J, Toyohara J, Fujita Y, Iyo M, Hashimoto K. Characterization of [3H]
876 CHIBA-1001 binding to α7 nicotinic acetylcholine receptors in the brain from rat, monkey, and
877 human. Brain research. 2010;1348:200-8.
878 59. Li Y-z, Liu X-h, Rong F, Hu S, Sheng Z-y. Carbachol inhibits TNF-α-induced endothelial
879 barrier dysfunction through alpha 7 nicotinic receptors. Acta Pharmacologica Sinica.
880 2010;31(10):1389-94.

881 60. Zhou G, Hu S, Lv Y, Song Q, Zou X, Sheng Z. Carbachol alleviates rat cytokine release
882 and organ dysfunction induced by lipopolysaccharide. Journal of Trauma and Acute Care
883 Surgery. 2011;71(1):157-62.
884 61. Halder N, Lal G. Cholinergic system and its therapeutic importance in inflammation and
885 autoimmunity. Frontiers in Immunology. 2021;12:660342.
886 62. Gray MA, Choy CH, Dayam RM, Ospina-Escobar E, Somerville A, Xiao X, et al.
887 Phagocytosis enhances lysosomal and bactericidal properties by activating the transcription
888 factor TFEB. Current Biology. 2016;26(15):1955-64.
889 63. Bantawa K, Sah SN, Subba Limbu D, Subba P, Ghimire A. Antibiotic resistance patterns
890 of Staphylococcus aureus, Escherichia coli, Salmonella, Shigella and Vibrio isolated from
891 chicken, pork, buffalo and goat meat in eastern Nepal. BMC research notes. 2019;12(1):1-6.
892 64. van den Honert MS, Gouws PA, Hoffman LC. A preliminary study: Antibiotic resistance
893 of Escherichia coli and Staphylococcus aureus from the meat and feces of various South African
894 wildlife species. Food Science of Animal Resources. 2021;41(1):135.
895 65. Liu J, Farmer Jr JD, Lane WS, Friedman J, Weissman I, Schreiber SL. Calcineurin is a
896 common target of cyclophilin-cyclosporin A and FKBP-FK506 complexes. Cell.
897 1991;66(4):807-15.
898 66. Najibi M, Labed SA, Visvikis O, Irazoqui JE. An evolutionarily conserved PLC-PKD-
899 TFEB pathway for host defense. Cell reports. 2016;15(8):1728-42.
900 67. LaValle CR, Bravo-Altamirano K, Giridhar KV, Chen J, Sharlow E, Lazo JS, et al. Novel
901 protein kinase D inhibitors cause potent arrest in prostate cancer cell growth and motility. BMC
902 chemical biology. 2010;10:1-16.

903 68. Carey K, Paulus G, Wang L, Balce D, Luo J, Bergman P, et al. TFEB transcriptional
904 responses reveal negative feedback by BHLHE40 and BHLHE41. Cell Rep 33: 108371. 2020.
905 69. Xu W-D, Li R, Huang A-F. Role of TL1A in inflammatory autoimmune diseases: a
906 comprehensive review. Frontiers in Immunology. 2022;13:891328.
907 70. Martina JA, Diab HI, Lishu L, Jeong-A L, Patange S, Raben N, et al. The nutrient-
908 responsive transcription factor TFE3 promotes autophagy, lysosomal biogenesis, and clearance
909 of cellular debris. Science signaling. 2014;7(309):ra9-ra.
910 71. Stumpo DJ, Lai WS, Blackshear PJ. Inflammation: cytokines and RNA-based regulation.
911 Wiley Interdisciplinary Reviews: RNA. 2010;1(1):60-80.
912 72. Makita S, Takatori H, Nakajima H. Post-transcriptional regulation of immune responses
913 and inflammatory diseases by RNA-binding ZFP36 family proteins. Frontiers in immunology.
914 2021;12:711633.
915 73. Jalonen U, Nieminen R, Vuolteenaho K, Kankaanranta H, Moilanen E, editors. Down-
916 regulation of tristetraprolin expression results in enhanced IL-12 and MIP-2 production and
917 reduced MIP-3alpha synthesis in activated macrophages. SCANDINAVIAN JOURNAL OF
918 IMMUNOLOGY; 2007: BLACKWELL PUBLISHING 9600 GARSINGTON RD, OXFORD
919 OX4 2DQ, OXON, ENGLAND.
920 74. Parrish WR, Rosas-Ballina M, Gallowitsch-Puerta M, Ochani M, Ochani K, Yang L-H, et
921 al. Modulation of TNF release by choline requires α7 subunit nicotinic acetylcholine receptor-
922 mediated signaling. Molecular medicine. 2008;14(9):567-74.
923 75. Peña G, Cai B, Liu J, van der Zanden EP, Deitch EA, de Jonge WJ, et al.
924 Unphosphorylated STAT3 modulates alpha7 nicotinic receptor signaling and cytokine production
925 in sepsis. European journal of immunology. 2010;40(9):2580-9.

926 76. Simon AR, Rai U, Fanburg BL, Cochran BH. Activation of the JAK-STAT pathway by
927 reactive oxygen species. American Journal of Physiology-Cell Physiology. 1998;275(6):C1640-
928 C52.
929 77. Liu J, Han X, Zhang T, Tian K, Li Z, Luo F. Reactive oxygen species (ROS) scavenging
930 biomaterials for anti-inflammatory diseases: from mechanism to therapy. Journal of Hematology
931 & Oncology. 2023;16(1):116.
932 78. Mao C, Li D, Zhou E, Zhang J, Wang C, Xue C. Nicotine exacerbates atherosclerosis
933 through a macrophage-mediated endothelial injury pathway. Aging (Albany NY).
934 2021;13(5):7627-43.
935 79. Tsoyi K, Jang HJ, Kim JW, Chang HK, Lee YS, Pae H-O, et al. Stimulation of alpha7
936 nicotinic acetylcholine receptor by nicotine attenuates inflammatory response in macrophages
937 and improves survival in experimental model of sepsis through heme oxygenase-1 induction.
938 Antioxidants & redox signaling. 2011;14(11):2057-70.
939 80. Su X, Lee JW, Matthay ZA, Mednick G, Uchida T, Fang X, et al. Activation of the α7
940 nAChR reduces acid-induced acute lung injury in mice and rats. American journal of respiratory
941 cell and molecular biology. 2007;37(2):186-92.
942 81. Lee RH, Vazquez G. Evidence for a prosurvival role of alpha-7 nicotinic acetylcholine
943 receptor in alternatively (M2)-activated macrophages. Physiol Rep. 2013;1(7):e00189.
944 82. St-Pierre S, Jiang W, Roy P, Champigny C, LeBlanc É, Morley BJ, et al. Nicotinic
945 acetylcholine receptors modulate bone marrow-derived pro-inflammatory monocyte production
946 and survival. PLoS One. 2016;11(2):e0150230.
947 83. Richter K, Grau V. Signaling of nicotinic acetylcholine receptors in mononuclear
948 phagocytes. Pharmacol Res. 2023;191:106727.

949 84. Lavin Y, Winter D, Blecher-Gonen R, David E, Keren-Shaul H, Merad M, et al. Tissue-
950 resident macrophage enhancer landscapes are shaped by the local microenvironment. Cell.
951 2014;159(6):1312-26.
952 85. Fujii T, Mashimo M, Moriwaki Y, Misawa H, Ono S, Horiguchi K, et al. Expression and
953 Function of the Cholinergic System in Immune Cells. Front Immunol. 2017;8:1085.
954 86. Lin Y-K, Yeh C-T, Kuo K-T, Fong I-H, Yadav VK, Kounis NG, et al. Apolipoprotein
955 (a)/Lipoprotein (a)-Induced oxidative-inflammatory α7-nAChR/p38 MAPK/IL-6/RhoA-GTP
956 signaling Axis and M1 macrophage polarization modulate inflammation-associated development
957 of coronary artery spasm. Oxidative medicine and cellular longevity. 2022;2022.
958 87. Khan MA, Farkhondeh M, Crombie J, Jacobson L, Kaneki M, Martyn JA.
959 Lipopolysaccharide upregulates alpha7 acetylcholine receptors: stimulation with GTS-21
960 mitigates growth arrest of macrophages and improves survival in burned mice. Shock.
961 2012;38(2):213-9.
962 88. Hernandez CM, Cortez I, Gu Z, Colón-Sáez JO, Lamb PW, Wakamiya M, et al. Research
963 tool: validation of floxed α7 nicotinic acetylcholine receptor conditional knockout mice using in
964 vitro and in vivo approaches. The Journal of physiology. 2014;592(15):3201-14.
965 89. Weiss FD, Alvarez Y, Sahu A, Shakeri F, Lee HE, Gellner A-K, et al. Retention of ES
966 cell-derived 129S genome drives NLRP1 hypersensitivity and transcriptional deregulation in
967 Nlrp3-/-mice. bioRxiv. 2024:2024.01. 03.573991.
968 90. Ito T, Inden M, Ueda T, Asaka Y, Kurita H, Hozumi I. The neuroprotective effects of
969 activated alpha7 nicotinic acetylcholine receptor against mutant copper-zinc superoxide
970 dismutase 1-mediated toxicity. Sci Rep. 2020;10(1):22157.

971 91. Li B, Wu J, Bao J, Han X, Shen S, Ye X, et al. Activation of alpha7nACh receptor
972 protects against acute pancreatitis through enhancing TFEB-regulated autophagy. Biochim
973 Biophys Acta Mol Basis Dis. 2020;1866(12):165971.
974 92. Martina JA, Chen Y, Gucek M, Puertollano R. MTORC1 functions as a transcriptional
975 regulator of autophagy by preventing nuclear transport of TFEB. Autophagy. 2012;8(6):903-14.
976 93. Ferron M, Settembre C, Shimazu J, Lacombe J, Kato S, Rawlings DJ, et al. A RANKL–
977 PKCβ–TFEB signaling cascade is necessary for lysosomal biogenesis in osteoclasts. Genes &
978 development. 2013;27(8):955-69.
979 94. Nabar NR, Heijjer CN, Shi C-S, Hwang I-Y, Ganesan S, Karlsson MC, et al. LRRK2 is
980 required for CD38-mediated NAADP-Ca2+ signaling and the downstream activation of TFEB
981 (transcription factor EB) in immune cells. Autophagy. 2022;18(1):204-22.
982 95. Hsu CL, Lee EX, Gordon KL, Paz EA, Shen W-C, Ohnishi K, et al. MAP4K3 mediates
983 amino acid-dependent regulation of autophagy via phosphorylation of TFEB. Nature
984 Communications. 2018;9(1):942.
985 96. Palmieri M, Pal R, Nelvagal HR, Lotfi P, Stinnett GR, Seymour ML, et al. mTORC1-
986 independent TFEB activation via Akt inhibition promotes cellular clearance in neurodegenerative
987 storage diseases. Nature communications. 2017;8(1):14338.
988 97. Martina JA, Jeong E, Puertollano R. p38 MAPK-dependent phosphorylation of TFEB
989 promotes monocyte-to-macrophage differentiation. EMBO reports. 2023;24(2):e55472.
990 98. Sha Y, Rao L, Settembre C, Ballabio A, Eissa NT. STUB 1 regulates TFEB-induced
991 autophagy–lysosome pathway. The EMBO journal. 2017;36(17):2544-52.

992 99. Li C, Wang X, Li X, Qiu K, Jiao F, Liu Y, et al. Proteasome inhibition activates
993 autophagy-lysosome pathway associated with TFEB dephosphorylation and nuclear
994 translocation. Frontiers in cell and developmental biology. 2019;7:170.

995

Figure 1

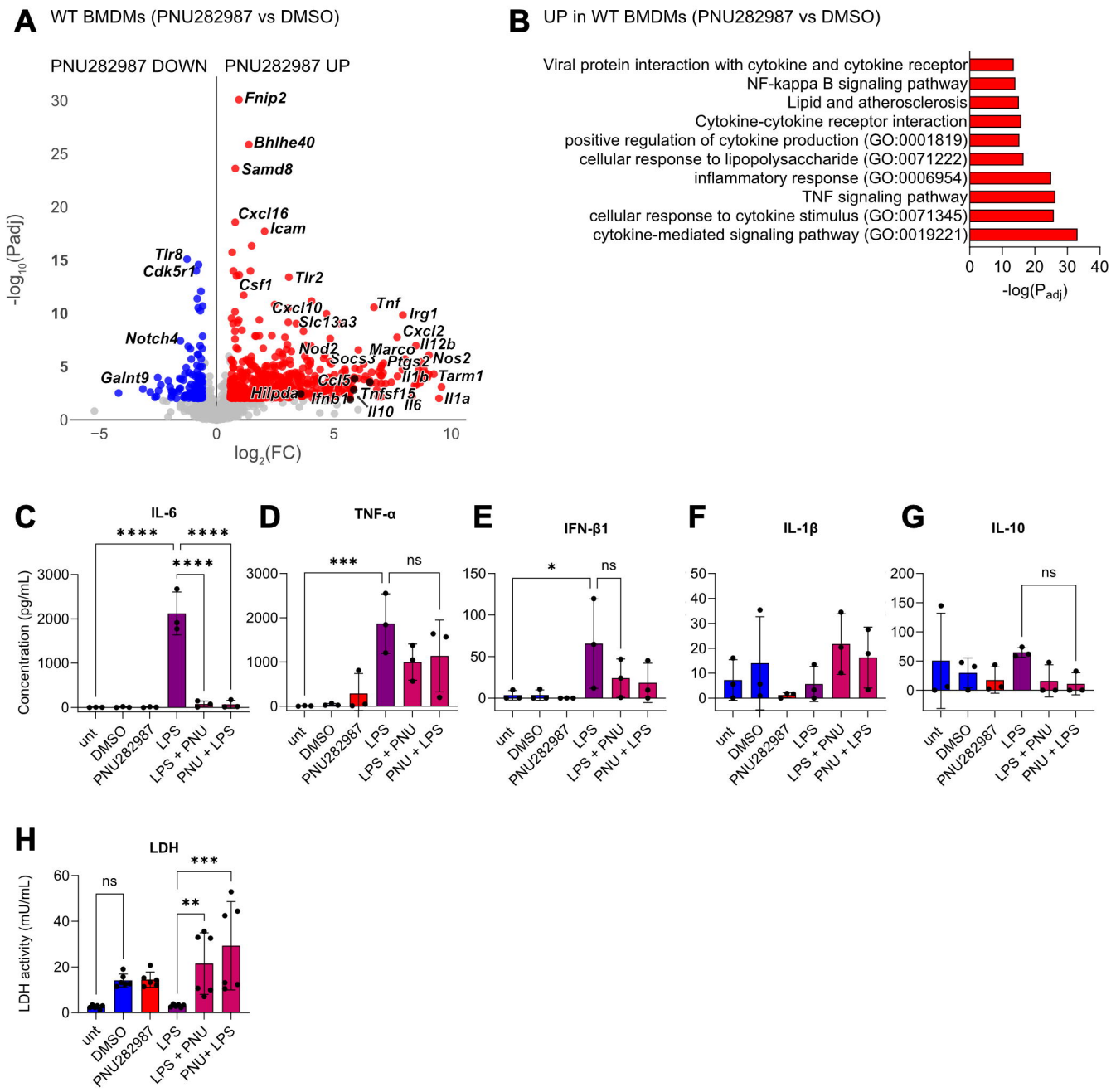
A
WT BMDMs (PNU282987 vs DMSO)
PNU282987 DOWN
PNU282987 UP
-log10(Padj)
log2(FC)
Fnip2
Bhlhe40
Samd8
Cxcl16
Icam
Tlr8
Cdk5r1
Csf1
Tlr2
Cxcl10
Slc13a3
Tnf
Irg1
Cxcl2
Il12b
Notch4
Nod2
Marco
Socs3
Ptgs2
Nos2
Galnt9
Ccl5
Il1b
Tarm1
Hilpda
Ifnb1
Tnfsf15
Il6
Il1a
Il10
B
UP in WT BMDMs (PNU282987 vs DMSO)
Viral protein interaction with cytokine and cytokine receptor
NF-kappa B signaling pathway
Lipid and atherosclerosis
Cytokine-cytokine receptor interaction
positive regulation of cytokine production (GO:0001819)
cellular response to lipopolysaccharide (GO:0071222)
inflammatory response (GO:0006954)
TNF signaling pathway
cellular response to cytokine stimulus (GO:0071345)
cytokine-mediated signaling pathway (GO:0019221)
-log(Padj)
C
IL-6
Concentration (pg/mL)
D
TNF-α
E
IFN-β1
F
IL-1β
G
IL-10
H
LDH
LDH activity (mU/mL)
unt
DMSO
PNU282987
LPS
LPS + PNU
PNU + LPS
ns

Figure 2

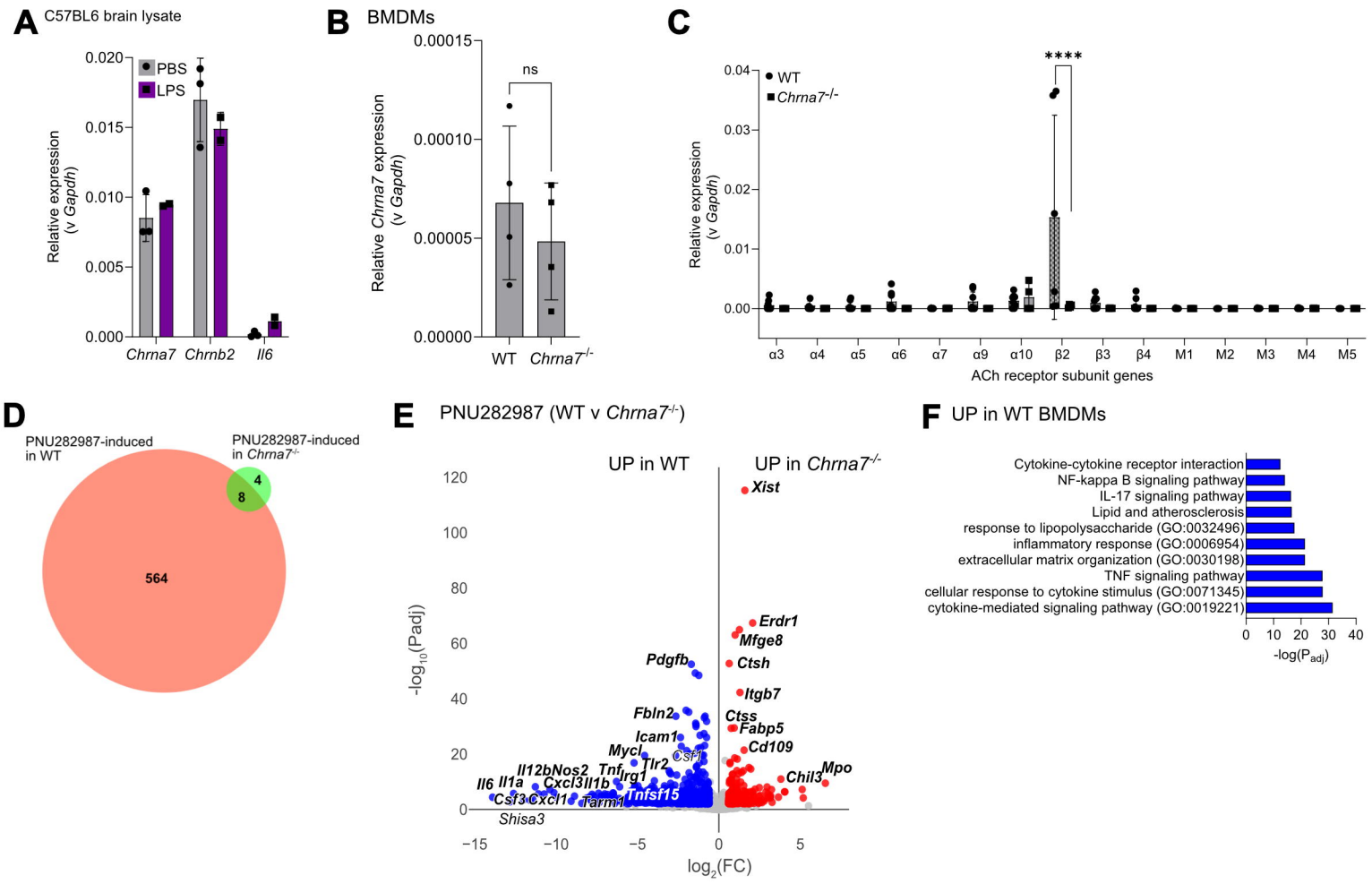
A
C57BL6 brain lysate
PBS
LPS
Relative expression (v Gapdh)
0.020
0.015
0.010
0.005
0.000
Chrna7
Chrnb2
Il6
B
BMDMs
Relative Chrna7 expression (v Gapdh)
0.00015
0.00010
0.00005
0.00000
ns
WT
Chrna7-/-
C
WT
Chrna7-/-
****
Relative expression (v Gapdh)
0.04
0.03
0.02
0.01
0.00
α3
α4
α5
α6
α7
α9
α10
β2
β3
β4
M1
M2
M3
M4
M5
ACh receptor subunit genes
D
PNU282987-induced in WT
PNU282987-induced in Chrna7-/-
564
8
4
E
PNU282987 (WT v Chrna7-/-)
UP in WT
UP in Chrna7-/-
-log10(Padj)
log2(FC)
Xist
Erdr1
Mfge8
Ctsh
Itgb7
Ctss
Fabp5
Cd109
Mpo
Chil3
Pdgfb
Fbln2
Icam1
Mycl
Tlr2
Csf1
Il12bNos2
Tnf
Irg1
Il6
Il1a
Cxcl3
Il1b
Tnfsf15
Csf3
Cxcl1
Tarm1
Shisa3
F
UP in WT BMDMs
Cytokine-cytokine receptor interaction
NF-kappa B signaling pathway
IL-17 signaling pathway
Lipid and atherosclerosis
response to lipopolysaccharide (GO:0032496)
inflammatory response (GO:0006954)
extracellular matrix organization (GO:0030198)
TNF signaling pathway
cellular response to cytokine stimulus (GO:0071345)
cytokine-mediated signaling pathway (GO:0019221)
-log(Padj)

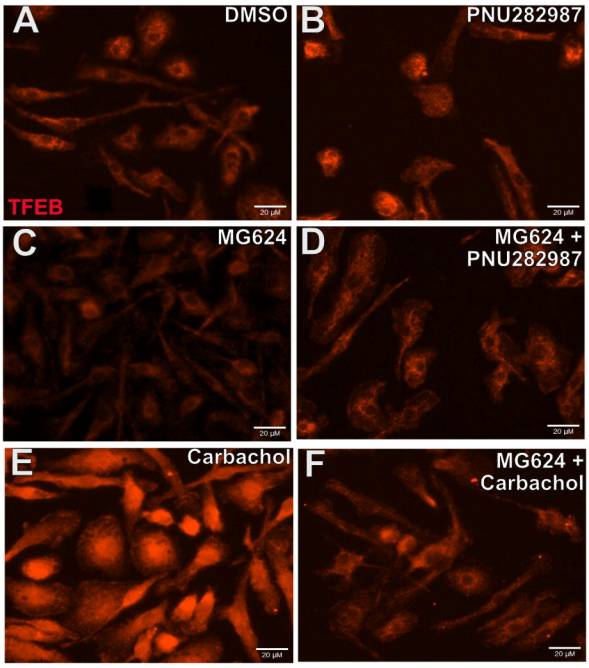
A
DMSO
TFEB
B
PNU282987
C
MG624
D
MG624 +
PNU282987
E
Carbachol
F
MG624 +
Carbachol

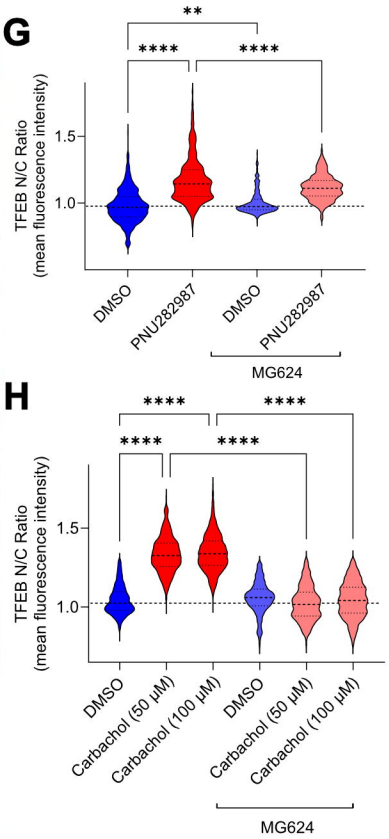
G
**
****
****
TFEB N/C Ratio
(mean fluorescence intensity)
1.5
1.0
DMSO
PNU282987
DMSO
PNU282987
MG624
H
****
****
****
****
TFEB N/C Ratio
(mean fluorescence intensity)
1.5
1.0
DMSO
Carbachol (50 μM)
Carbachol (100 μM)
DMSO
Carbachol (50 μM)
Carbachol (100 μM)
MG624

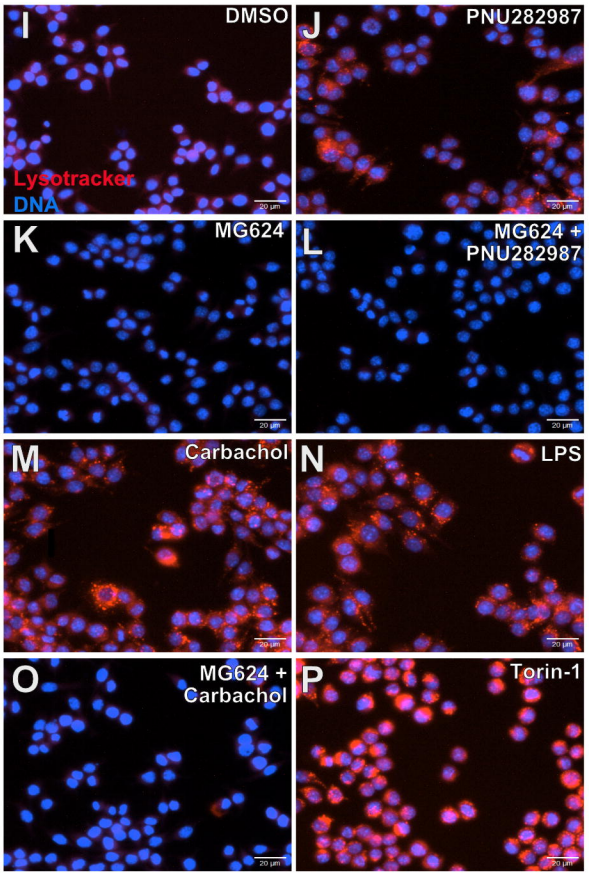
I
DMSO
Lysotracker
DNA
J
PNU282987
K
MG624
L
MG624 +
PNU282987
M
Carbachol
N
LPS
O
MG624 +
Carbachol
P
Torin-1

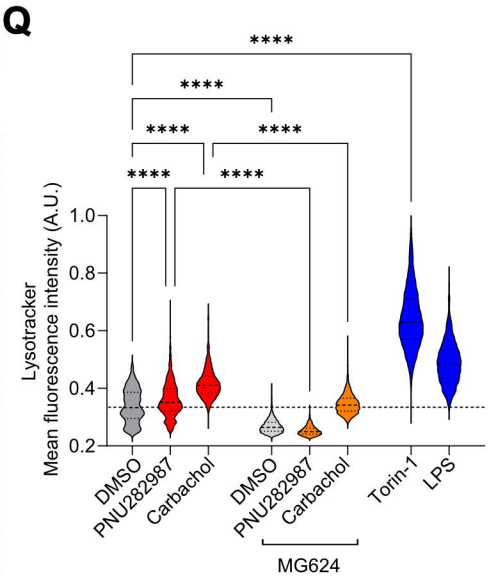
Q
****
****
****
****
****
****
Lysotracker
Mean fluorescence intensity (A.U.)
1.0
0.8
0.6
0.4
0.2
DMSO
PNU282987
Carbachol
DMSO
PNU282987
Carbachol
Torin-1
LPS
MG624

Figure 4

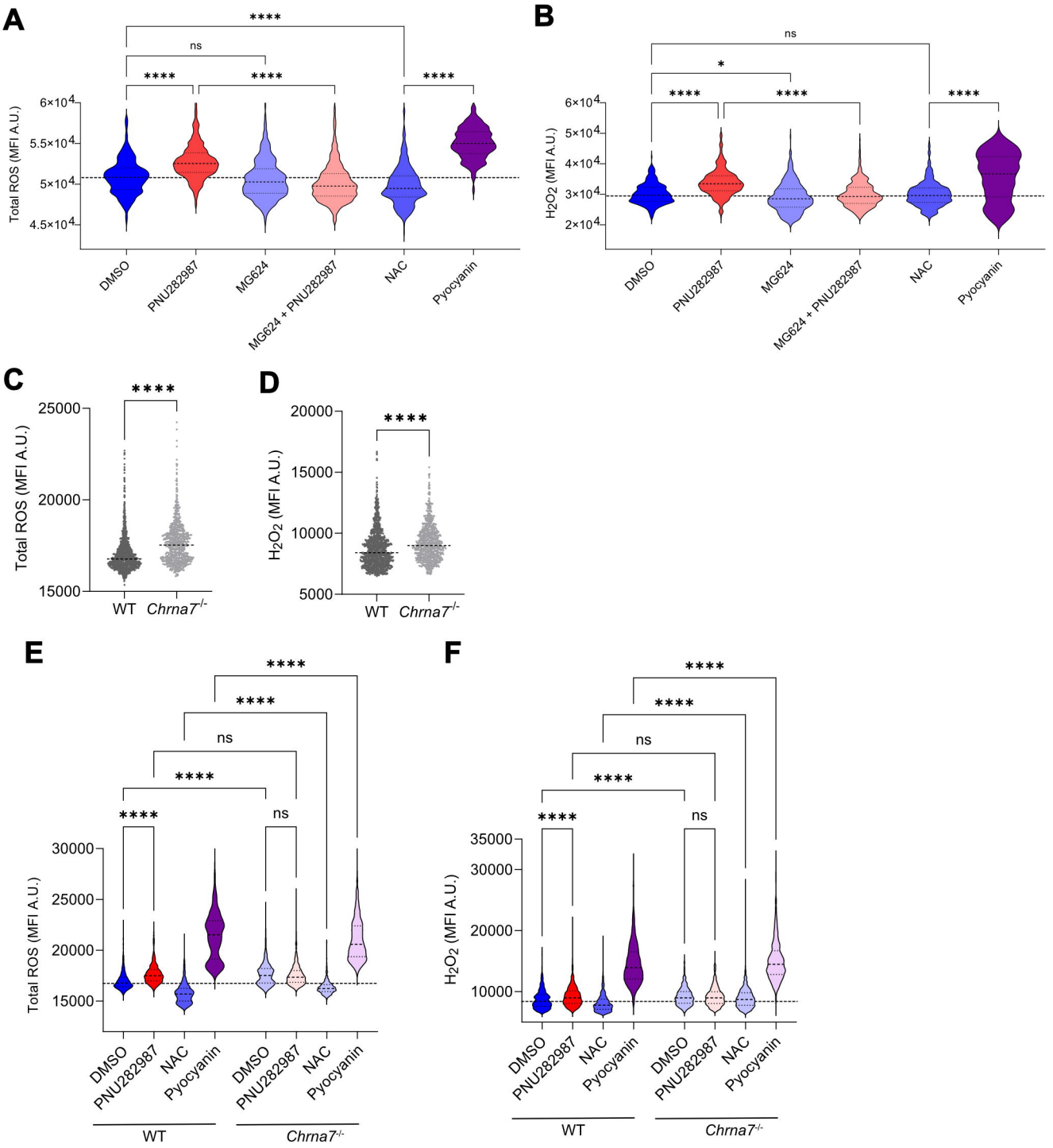
A
Total ROS (MFI A.U.)
6×10^4
5.5×10^4
5×10^4
4.5×10^4
****
ns
****
****
****
DMSO
PNU282987
MG624
MG624 + PNU282987
NAC
Pyocyanin
B
H2O2 (MFI A.U.)
6×10^4
5×10^4
4×10^4
3×10^4
2×10^4
ns
*
****
****
****
DMSO
PNU282987
MG624
MG624 + PNU282987
NAC
Pyocyanin
C
Total ROS (MFI A.U.)
25000
20000
15000
****
WT
Chrna7-/-
D
H2O2 (MFI A.U.)
20000
15000
10000
5000
****
WT
Chrna7-/-
E
Total ROS (MFI A.U.)
30000
25000
20000
15000
****
****
ns
****
****
ns
DMSO
PNU282987
NAC
Pyocyanin
DMSO
PNU282987
NAC
Pyocyanin
WT
Chrna7-/-
F
H2O2 (MFI A.U.)
35000
30000
20000
10000
****
****
ns
****
****
ns
DMSO
PNU282987
NAC
Pyocyanin
DMSO
PNU282987
NAC
Pyocyanin
WT
Chrna7-/-

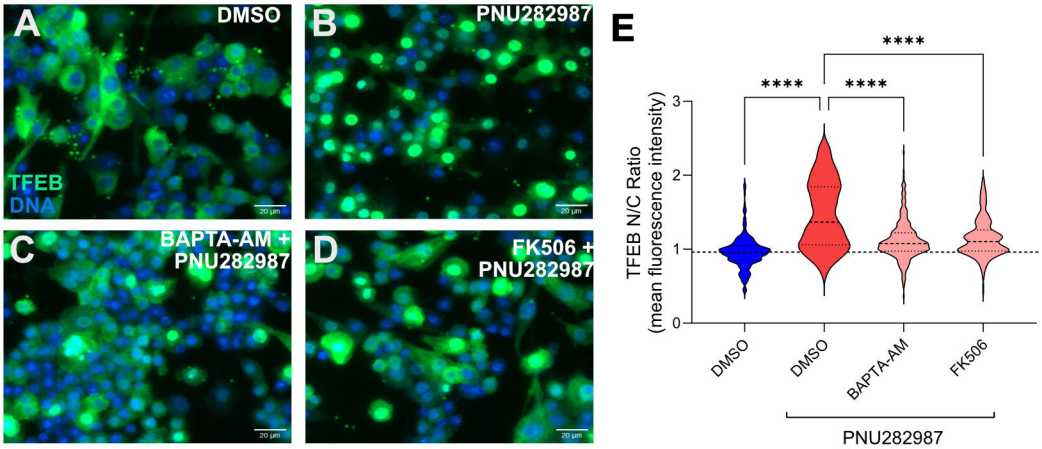
A
DMSO
TFEB
DNA
B
PNU282987
C
BAPTA-AM +
PNU282987
D
FK506 +
PNU282987
E
****
****
****
TFEB N/C Ratio
(mean fluorescence intensity)
0
1
2
3
DMSO
DMSO
BAPTA-AM
FK506
PNU282987

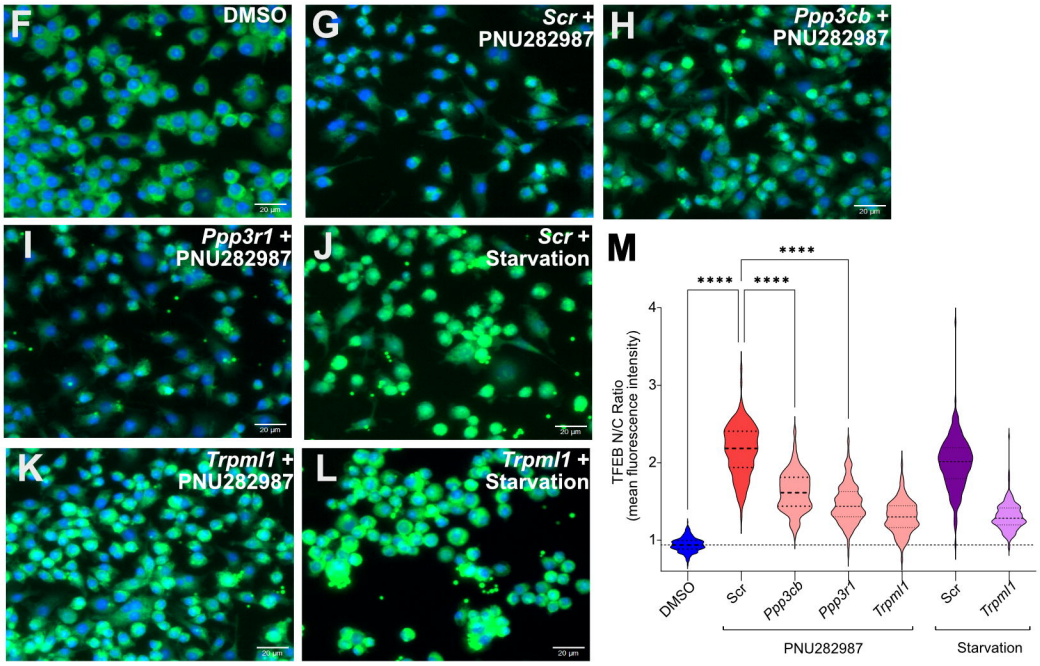
F
DMSO
G
Scr +
PNU282987
H
Ppp3cb +
PNU282987
I
Ppp3r1 +
PNU282987
J
Scr +
Starvation
K
Trpml1 +
PNU282987
L
Trpml1 +
Starvation
M
****
****
****
TFEB N/C Ratio
(mean fluorescence intensity)
1
2
3
4
DMSO
Scr
Ppp3cb
Ppp3r1
Trpml1
Scr
Trpml1
PNU282987
Starvation

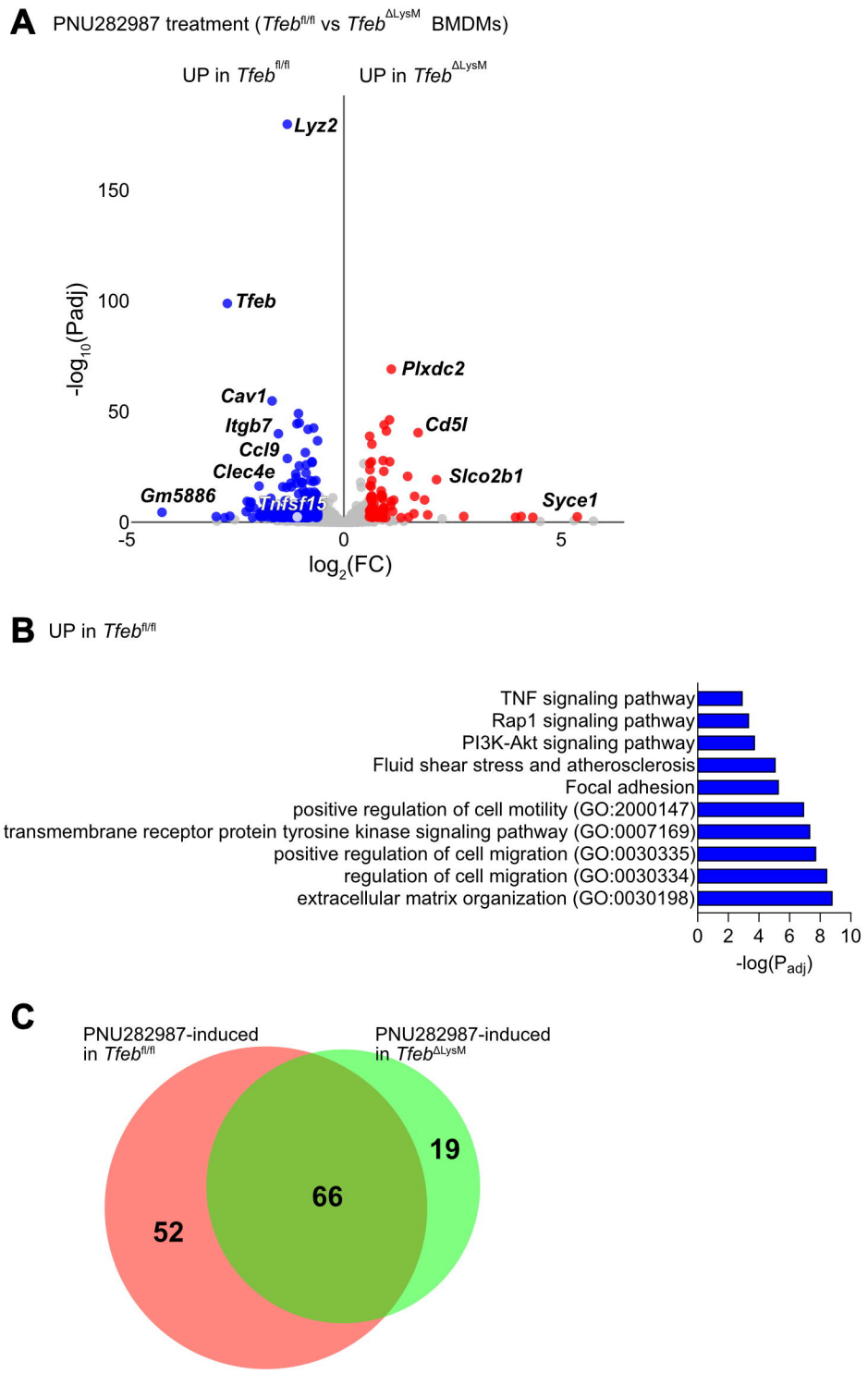
A
PNU282987 treatment (Tfeb fl/fl vs Tfeb ΔLysM BMDMs)
UP in Tfeb fl/fl
UP in Tfeb ΔLysM
Lyz2
Tfeb
Cav1
Itgb7
Ccl9
Clec4e
Gm5886
Tnfsf15
Plxdc2
Cd5l
Slco2b1
Syce1
-log10(Padj)
log2(FC)
B
UP in Tfeb fl/fl
TNF signaling pathway
Rap1 signaling pathway
PI3K-Akt signaling pathway
Fluid shear stress and atherosclerosis
Focal adhesion
positive regulation of cell motility (GO:2000147)
transmembrane receptor protein tyrosine kinase signaling pathway (GO:0007169)
positive regulation of cell migration (GO:0030335)
regulation of cell migration (GO:0030334)
extracellular matrix organization (GO:0030198)
-log(Padj)
C
PNU282987-induced in Tfeb fl/fl
PNU282987-induced in Tfeb ΔLysM
52
66
19